was described as a percentage of wild-type pig fibroblasts, which was calculated as follows; Percentage of αGal expression level = (MFI of cloned pig with FITC-labeled GS-IB4 – MFI of positive control without FITC-labeled GS-IB4)/(MFI of positive control with FITC-labeled GS-IB4 – MFI of positive control without FITC-labeled GS-IB4) × 100.

Anti-pig antibody levels in baboon sera were also examined by flow cytometry using donor pig red blood cells. FITC-labeled rabbit anti-human IgM or IgG antibodies (Dako, Glostrup, Denmark) were used as a second antibody after reaction of recipient sera with pig red blood cells as described previously [23,31].

Polymerase chain reaction analysis of transgenes

The transgene of hDAF was detected in transfected cells, tissue from cloned piglets and tissues from progeny by PCR with a 20-base sense primer 5′-AAGGCCGTACAAGTTTTCCC-3′, and a 20-base antisense primer 5′-GAACTGTTTGGGGGACCTTG-3′. Amplification conditions were initial denaturation at 94 °C for 5 min followed by 40 cycles of denaturation at 94 °C for 1 min, annealing at 60 °C for 1 min and extension at 72 °C for 1 min, and a final extension for 5 min at 72 °C. The amplified product was a 741-base pair (bp) fragment. The transgene of EndoGalC was detected in transfected cells, tissue from cloned piglets and tissues from progeny by PCR with two sets of primers 5′-TTACATCCAGATTCAGCAAC-3′, 5′-GGAACATTAGCCATAACTTC-3′ and 5′-TAGAGACACAAGTTGGAGATGGT-3′, 5′-GCTAATTGAATATCAGTATTTTTCAC-3′. Amplification conditions were initial denaturation at 94 °C for 5 min followed by 40 cycles of denaturation at 94 °C for 1 min, annealing at 55 °C for 1 min and extension at 72 °C for 1 min. A final extension for 5 min at 72 °C was incubated after the cycle. The amplified products were 470- and 700-bp fragment. PCR products were analyzed by electrophoresis on a 1.0% agarose gel and visualized under UV illumination after staining gels with ethidium bromide.

Immunohistochemical staining of organs from cloned pigs

Biopsies of cloned pig heart, kidney and liver were formalin-fixed for hematoxylin-eosine staining and quickly frozen in liquid nitrogen and stored at −80 °C in preparation for immunohistochemical studies. The expression of hDAF and αGal was examined using FITC-labeled mouse anti-human CD55 antibody and FITC-labeled GS-IB4 lectin. Deposition of antibody, complement, and fibrinogen on the transplanted pig kidneys was identified using FITC-conjugated rabbit antibodies to human IgG, IgM, C3, and fibrinogen (Dako).

Pig to baboon kidney transplantation

Genetically engineered pigs expressing hDAF or both hDAF and EndoGalC weighing 20 to 26 kg, and baboons (Papio anubis or Papio hamadryas) weighing 11 to 23 kg were used as donors and recipients, respectively. Recipient baboon was anesthetized using ketamine and maintained on inhaled halothane or sevoflurane and oxygen. A left or right kidney, which was typically excised from a donor pig, was transplanted into the abdominal cavity of a recipient baboon. The donor aorta with renal artery and renal vein were anastomosed end-to-side to the recipient aorta and inferior vena cava. After ureteroureterostomy was performed, the inserted ureteral stent catheter was brought out through the bladder and the subcutaneous tunnel onto the lower back, which allowed monitoring of urine output. The spleen was removed immediately before transplantation. Biopsies of kidney grafts were routinely conducted pre- and 1 h-post-transplantation. Excised grafts from euthanized baboons at the end of the experiment were also examined for immunohistochemical study. As described in Table 1, a total of

Table 1. Pig to baboon renal transplantation

Recipient baboon	IgM[a]	IgG[a]	Donor cloned pig	Gal expression[b]	hDAF expression[c]	Tissue sample
B0501[d]	35	8	hDAF + EndoGalC (DE-45)	2	45-fold	1 h, 3 days, 7 days, 8 days (AVR)
B0603	66	12	hDAF + EndoGalC (DE-400)	3	11-fold	1 h, 11 days (AVR)
B0705	74	2	hDAF + EndoGalC (DE-107)	14	25-fold	1 h, 9 days (Pyelonephritis)
B0602	51	16	hDAF + EndoGalC (DE-399)	8	27-fold	1 h, 2 days[e] (Normal)

[a]IgM and IgG binding level was expressed as a percentage of human pooled sera bound to wild-type pig cells.
[b]Gal expression level was expressed as a percentage of wild-type pig fibroblasts.
[c]hDAF expression level was expressed as a relative value of human positive control (HUVEC or HAEC).
[d]One native kidney was left (NOT life supporting model), because of frequent graft biopsy.
[e]Baboon died due to the arterial line trouble with functioning graft.

four pig kidneys were engrafted into the baboons. All recipients underwent bilateral nephrectomy immediately after transplantation except B0501 in which one native kidney was preserved because of frequent graft biopsy after transplantation.

Immunosuppression

Immunosuppressive protocol included clinically acceptable drugs such as tacrolimus (0.5 mg/kg/day, i.m. day-1 and 0.1 mg/kg/day, i.v.), cyclophosphamide (2 mg/kg/day, i.m. day-1 and 1 mg/kg/day, i.v.) and methylprednisolone (125 mg, i.v. day 0 and then tapered). Penicillin and cephem antibiotics were administered every 12 h. After operation, baboons were treated with buprenorphine hydrochloride. No anti-pig antibody removal procedure such as plasmapheresis or immunoadsorption was performed before transplantation.

Results

Expression level of genetically engineered cloned pigs expressing hDAF

After fetal fibroblasts into which the hDAF expression vector was introduced were selected by puromycin, living cells were collectively expanded. The expanded cells were sorted within the range of M1 by FACS, so cell mass with high hDAF expression was obtained (Fig. 2A). From cloned embryos that had been derived from the nuclear transfer of hDAF expressing cells transferred to surrogate mothers, two cloned piglets (cloned pigs-1D and -2D) were safely born. Analysis of genomic DNA from these cloned piglets by PCR indicated that both of them had hDAF gene (data not shown). However, as one piglet (cloned pig-2D) died in 1 week because of an accident, the aortic endothelial cells were harvested immediately after death. Fibroblasts obtained from the ear of two cloned piglets were subjected to flow cytometric analysis for evaluation of the hDAF expression level. Fibroblasts were found to express about 20- to 30-fold higher hDAF compared to HAEC (Fig. 3). Endothelial cells expressed over 80-fold hDAF as a relative value of human control (HUVEC). Endothelial cells appeared to show higher expression of hDAF than fibroblasts. Immunohistochemical staining for hDAF of heart, kidney, and liver sections from cloned pig-2D demonstrated very high expression in endothelial cells (Fig. 4).

Inhibition of αGal expression in cloned pigs expressing EndoGalC

EndoGalC-expressed cells, namely, with a low level of αGal expression, were obtained in the same way as high hDAF-expressing cells using a cell sorter (Fig. 2B). From cloned embryos that had been derived from the nuclear transfer of EndoGalC expressing cells transferred to surrogate mothers, three cloned piglets (cloned pigs-1E, 2E and 3E) were safely born without any deformity. However, all piglets died from inadequate nursing by its mother, pneumonia and an accident occurred within 0 to 45 days postnatally. The fourth cloned piglet (cloned pig-4E, female) successfully grew to maturity and produced progeny. EndoGalC gene was confirmed to be present in all the cloned pigs by genomic PCR analysis (data not shown). Flow cytometric analysis demonstrated that the αGal expression level in fibroblasts from the first two cloned piglets (cloned pig-1E, 2E) and fourth cloned piglet (cloned pig-4E) was effectively reduced by over 98% (Fig. 5). Immunohistochemical staining for αGal antigens of heart and kidney sections from cloned pig-2E demonstrated that αGal expression was reduced to undetectable levels (Fig. 6). Genomic PCR analysis revealed successful incorporation (transmission) of hDAF

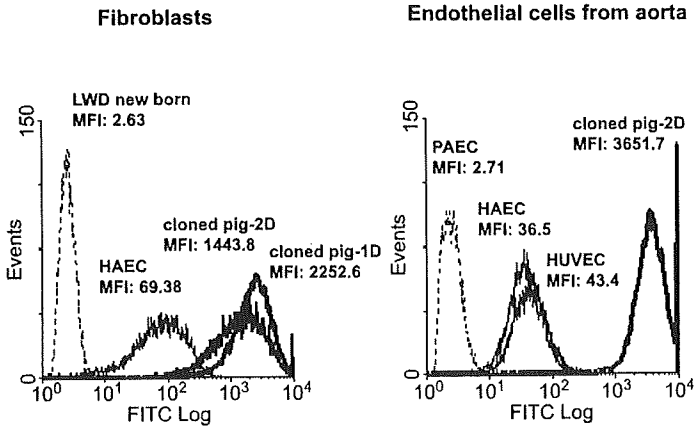

Fig. 3. Flow cytometric analysis of fibroblasts and aortic endothelial cells from cloned piglets expressing hDAF. Left panel: fibroblasts; right panel: endothelial cells. Mean fluorescence intensity (MFI) levels are indicated. Cloned pig-1D and -2D (thick lines) were compared with negative controls (fibroblasts and PAEC from wild-type pigs indicated by dashed line) and positive controls (HAEC and HUVEC indicated by thin lines). Fibroblasts of cloned pig-1D and -2D expressed 32-fold and 21-fold of hDAF compared with HAEC, respectively. Endothelial cells of cloned pig-2D expressed over 80-fold compared with HUVEC.

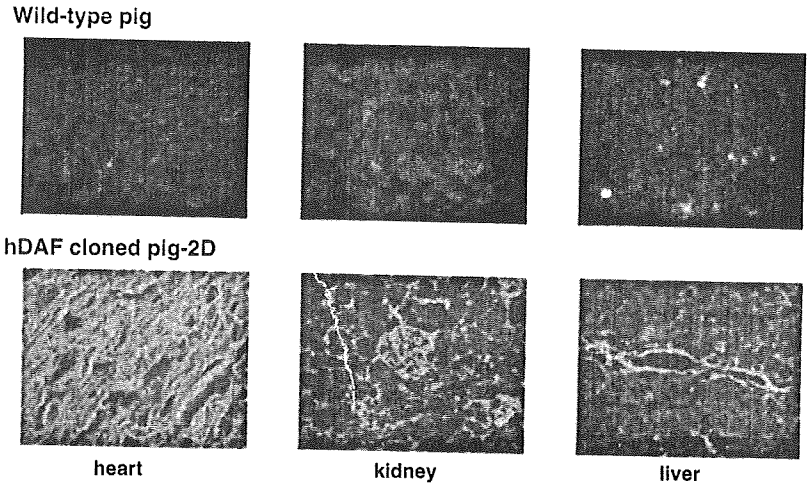

Fig. 4. Immunohistochemical staining of organs from cloned pig expressing hDAF. Organs were retrieved from dead cloned pig-2D expressing hDAF. Top panels: wild-type pig as a control; bottom panels: cloned pig expressing hDAF. Left: heart; middle: kidney; right: liver. Vascular endothelial cells show strong staining for hDAF. It was noted that hDAF was specifically expressed in the regions of peritubular capillaries and glomeruli of kidney.

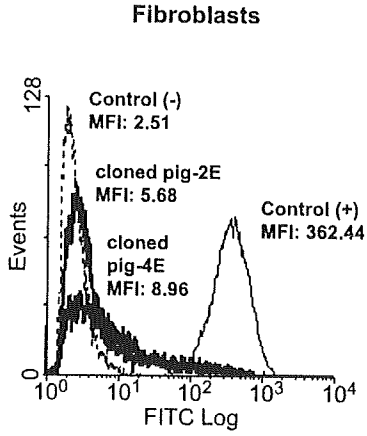

Fig. 5. Flow cytometric analysis of fibroblasts from cloned piglets expressing EndoGalC. Cloned pig-2E and 4E (thick lines) were compared with positive controls (fibroblasts from wild-type pigs indicated by thin line). αGal antigens were almost completely removed in cloned pigs. Percentages of αGal expression in cloned pigs were about 1 to 2% of that in wild-type pig. Negative control (control (−)) was unstained fibroblasts from wild-type pigs, which was indicated by dashed line.

and EndoGalC transgenes (data not shown). RT-PCR analysis of various organs such as heart, lung, kidney, liver, pancreas, spleen, and small intestine from cloned pigs also showed expression of hDAF or EndoGalC mRNA (data not shown).

Cross-breeding of cloned pigs expressing hDAF and EndoGalC

F1 pigs were born from hDAF cloned pig-1D and EndoGalC cloned pig-4E (Fig. 7). After careful cross-breeding, a total of 38 F1, 38 F2 and 27 F3 pigs were produced. There was no obvious increase of stillbirth and no problem in growth rate or in sexual maturation. In addition, no difference was especially observed among F1, F2, and F3 generations, though a tendency to smaller litter size was observed compared to non-transgenic pigs. The expression level of hDAF and αGal fluctuated to some degree. Although the efficacy of αGal reduction dropped after F1 generation, the expression of αGal antigens was maintained at relatively low levels of about 2 to 14% compared with wild-type pigs. The expression of hDAF also showed individual differences. By retaining only pigs with a high level of expression, stable transmission of transgene expression to progeny was obtained.

Pig to baboon renal transplantation

Four genetically engineered pig kidneys were transplanted into baboons in the present study (Table 1). IgM and IgG levels bound to red blood cells from donor pig in recipient baboon sera were represented as a percent of human control sera, which were attached to red blood cells from wild-type pig.

All baboon sera contained a similar level of anti-pig IgM (35 to 74%) and a very low level of IgG (2 to 16%), when compared with human control sera. Anti-donor IgM levels in baboons were not much reduced even when EndoGalC cloned pigs were used as donors, because of the small amount of remaining αGal and immunogenic non-Gal epitopes. In contrast, as baboons tended to have a considerably lower level of IgG than humans, anti-donor IgG levels in all recipient baboons were below 20%.

In B0501, one native kidney was left after transplantation, because of frequent graft biopsy. Hyperacute rejection was not observed. Graft biopsy was conducted 1 h, 3 days, and 7 days after transplantation. Baboon was euthanized on day 8, because of deterioration in the general condition due to bleeding. Macroscopically, the excised graft showed neither the bleeding nor the necrosis characteristic of severe acute vascular rejection. However, microthrombi in glomeruli were detected

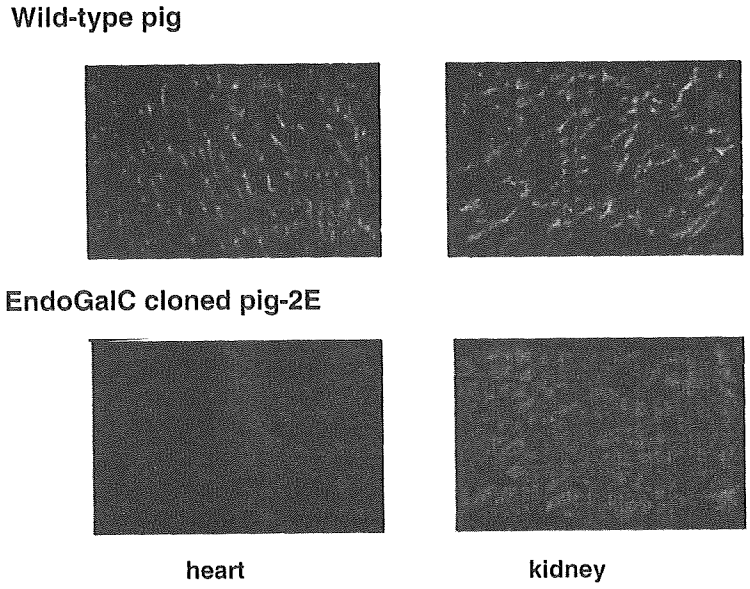

Fig. 6. Immunohistochemical staining of organs from cloned pig expressing EndoGalC. Organs were retrieved from dead cloned pig-2E expressing EndoGalC. Top panels: wild-type pig as a control; bottom panels: cloned pig expressing EndoGalC. Left: heart; right: kidney. Cloned pig organs express αGal antigens at negligible levels.

on day 7 and diffusely observed on day 8 (Fig. 8). Immunohistochemical analysis revealed obvious deposition of IgM, IgG, C3, and fibrinogen 1 h after transplantation (Fig. 9). Strong deposition of IgM was maintained, while IgG was attached at a low level, probably due to the low level of anti-pig IgG in recipient baboon sera. The binding of IgG and C3 decreased to a low or undetectable level after day 3. In contrast, depositions of IgM and fibrinogen were strongly detected until graft excision on day 8.

Neither B0603, B0705 nor B0602 showed hyperacute rejection. Anti-pig antibodies dropped immediately after transplantation and maintained low levels (due to the graft absorption) until graft removal. B0603 and B0705 were euthanized due to the increase of serum creatinine on day 11 and 9, respectively. The excised graft in B0603 showed bleeding and necrosis in the cortical region. Histopathology demonstrated interstitial cell infiltration, inflammation in arteries and widespread thrombosis in glomeruli, by which acute vascular rejection was characterized. The graft in B0705 showed mononuclear cell and mainly granulocyte infiltration in the lumen of tubules, but no endothelial damage in glomeruli, which suggested pyelonephritis because of isolation of Enterobacter cloacae from blood culture. However, microthrombi in glomeruli were also detected as in other cases. Although the condition of B0602 was very good after transplantation, cerebral embolism due to arterial line trouble was suspected to happen on day 2. Since the baboon in this case suffered from low blood pressure and convulsion, the animal was euthanized. The excised

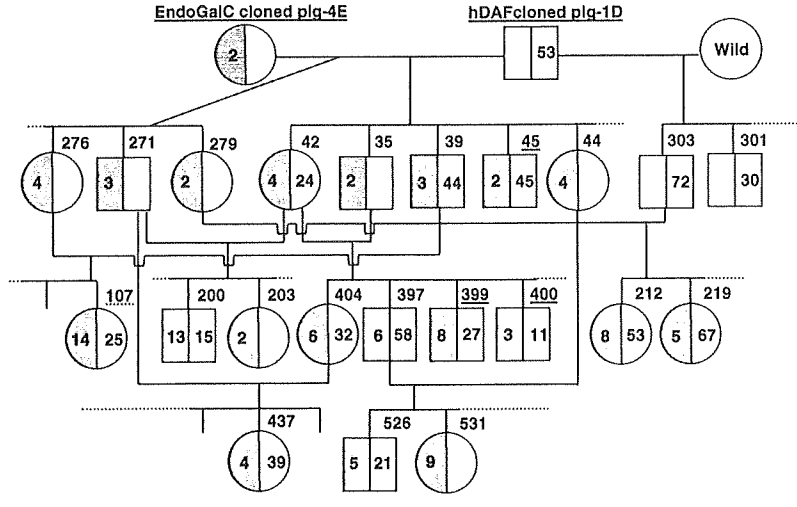

Fig. 7. Cross-breeding of hDAF and EndoGalC expressing pigs. The course of cross-breeding of pigs expressing hDAF and EndoGalC is depicted. Circle and square indicate female and male pig, respectively. Pig number is expressed above the circle or square. Pigs with underlined number were used as donors for transplantation experiment in the present study. Gray and blank show successful transgene expression and no transgene, respectively. Values on the left and right side of circles and squares indicate αGal expression level in fibroblasts (percentage of wild-type pig fibroblasts) and hDAF expression level in fibroblasts (multiples of human positive control, HUVEC or HAEC), respectively.

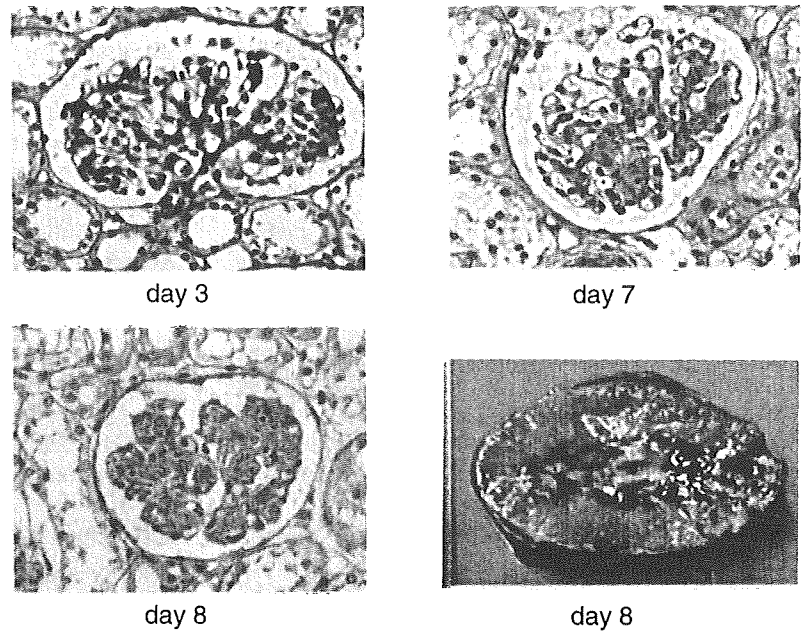

Fig. 8. Histopathology of graft biopsy (B0501). Almost normal findings were observed on day 3 (left top). Slight microthrombi on day 7 (right top) developed into widespread thrombus formation in glomeruli on day 8 (left bottom). Tubules were almost normal. No hemorrhagic or necrotic lesion was macroscopically found in graft (right bottom).

graft showed almost normal finding both macroscopically and microscopically (data not shown).

Discussion

Using the pig cloning technology we originally developed [25,32], we successfully produced two transgenic pigs. In this study, for pig to non-human primate transplantation, we utilized genetically engineered pigs expressing both hDAF and EndoGalC at the F1 generation immediately after cross-breeding from F0 parent pigs (father with hDAF and mother with EndoGalC). After cross-breeding, the αGal expression level increased from below 2% in F0 to 2–14% in F1 and later generations. In contrast, hDAF expression was maintained at high levels, despite some fluctuation. It has been speculated that the incorporated site of hDAF might be limited to one region, while EndoGalC transgene has been inserted at several functioning sites. Although littermates were considerably fewer (one to three) in the production of cloned pigs than

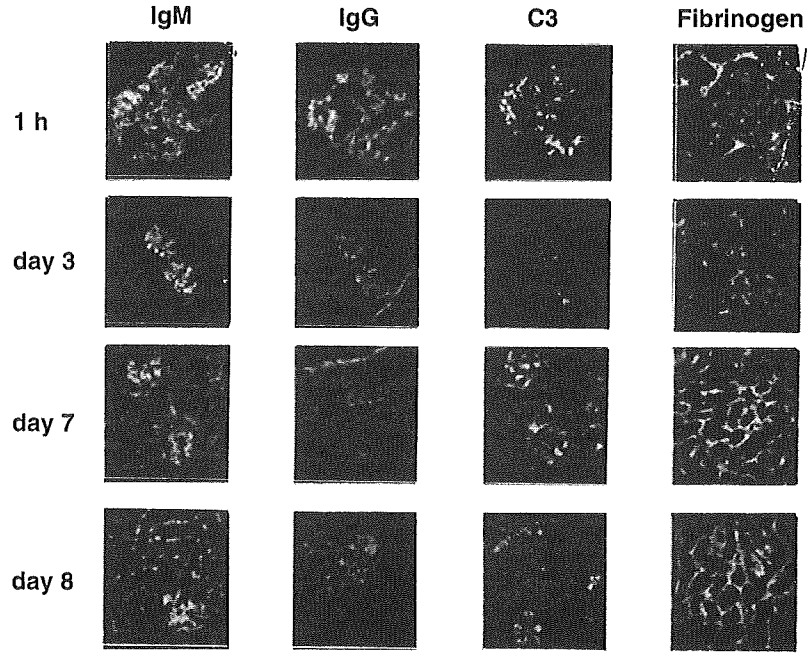

Fig. 9. Immunohistochemical staining of graft biopsy (B0501).Graft biopsy sections obtained at 1 h, and on days 3, 7 and 8, were stained for IgM, IgG, C3, and fibrinogen. All of IgM, IgG, C3, and fibrinogen were detected 1 h after transplantation. IgG and C3 deposition levels were maintained at a low level. In contrast, strong staining of IgM and fibrinogen was observed through this experiment. Fibrinogen staining became even stronger on days 7 and 8 (original magnification 200×).

in non-transgenic pigs, they recovered to the regular size (around 10) during cross-breeding. No congenital deformity nor growth retardation was observed in our cloned pigs expressing hDAF and EndoGalC. Although the fluctuation of transgene expression levels might be caused by the delicate assay method to some extent, the reduction of transgene expression may also be ascribed to epigenetic factors and probably would not be passed down to progeny. However, since a possibility of transmission of such reduced expression to progeny cannot be completely ruled out, it might be preferable to quantify the level of phenotypic transformation (i.e., the expression level of hDAF and αGal measured by flow cytometry) in all produced piglets and to keep only the suitable piglets for production of progeny.

When both hDAF- and EndoGalC-expressed kidneys were transplanted into baboons without antibody removal, hyperacute rejection could be avoided in four naive baboons containing anti-pig antibodies at the level below human control sera. hDAF expression at a high level is acknowledged to be very effective for preventing hyperacute rejection, but graft function was steadily aggravated in a week. In this study, graft biopsy revealed almost normal findings on day 3, but scanty microthrombi formation in glomeruli on day 7 and diffused microthrombi on day 8. Immunohistochemical study demonstrated that fibrinogen was detected as early as 1 h after transplantation. It was suggested that a graft might lapse into the procoagulant state due to antibody binding immediately after transplantation, even when a kidney expressing a high level of hDAF expression was used. C3 deposition, which was clearly observed 1 h after reperfusion, was reduced and maintained at very low levels. Weak expression of hDAF during cold preservation might make a recovery and exhibit effective function of complement inhibition with time.

Although effective inhibition of complement activation could be accomplished by a high level of hDAF transgene as was shown to almost completely inhibit cytotoxicity of human and baboon sera in our previous in vitro test [22], sufficient antibody binding could elicit a procoagulant state step by step, and eventually cause acute vascular rejection. Antibody-induced complement activation not only inflicts injury on cell membrane, but also would be a main initiator for endothelial cell activation and procoagulation. The anti-pig cytotoxicity level in recipient sera, which is considered to be indicative of hyperacute rejection, might be too insensitive for acute vascular rejection. Although there is a possibility of some difference in the antibody binding level among donor RBC, endothelial cells and fibroblasts, the development of an assay method to evaluate antibody binding, complement activation and the procoagulant activity in a comprehensive way would be preferable.

In the present study, a genetically engineered pig expressing only EndoGalC was not used as a donor, because the beneficial effect of incomplete αGal elimination on graft survival can not be expected due to the antibody reaction against the remaining αGal antigens. Pig cells with removal of 99% of αGal antigens by EndoGalC certainly caused a strong immune response and anti-Gal antibody production [33], so complete elimination of αGal antigens is essential. The effect of EndoGalC expression on Gal reduction seems to be more potent than another alternative strategy to GT-KO such as α 1,2 fucosyltransferase [34] or *N* acetylglucosaminyltransferase-III [35]. However, when GT-KO pigs are available, EndoGalC gene transfer would be unnecessary, although there remains a small possibility that the expression of EndoGalC might be required as an additional strategy to GT-KO, if a specific αGal epitope happens to be newly expressed.

In conclusion, (i) two types of cloned pigs with a very high level of hDAF expression and a low level of αGal expression by EndoGalC transgene were produced by collection of highly expressed transfected cells using a cell sorter, and somatic cell nuclear transfer. (ii) Pedigree breeding of genetically engineered pigs with stable expression of both hDAF and EndoGalC was established by cross-breeding. (iii) In a pig to naive baboon renal transplantation model, hyperacute rejection can be avoided without pretreatment of antibody removal. (iv) Fibrinogen was detected as early as 1 h after reperfusion and microthrombi in glomeruli were diffusely extended in 1 week. (v) Suppression of antibody binding to the graft would be required, even if a high level of hDAF is expressed.

Acknowledgments

The authors thank Ms. Yuriko Sawa, Ms. Naoko Asano, Ms. Misao Niwa and Mr. Ma Liang for their excellent technical assistance and Drs. Takahisa Hiramitsu, Shuichi Shimabukuro, Takayuki Yamamoto, and Akio Katayama for their skillful transplant surgery. This study was supported by Grants-in-Aid for Scientific Research (No. 18591407 and No. 20390340) from the Japan Society for the Promotion of Science (KAKENHI) and Research Grant (Integrated Research Project for Plant, Insect and Animal using Genome Technology) from the Ministry of Agriculture, Forestry and Fisheries of Japan.

References

1. PHELPS CJ, KOIKE C, VAUGHT TD et al. Production of alpha 1,3-galactosyltransferase-deficient pigs. Science 2003; 299: 411–414.
2. KOLBER-SIMONDS D, LAI LX, WATT SR et al. Production of alpha-1,3-galactosyltransferase null pigs by means of nuclear transfer with fibroblasts bearing loss of heterozygosity mutations. Proc Natl Acad Sci USA 2004; 101: 7335–7340.
3. NOTTLE MB, BEEBE LFS, HARRISON SJ et al. Production of homozygous alpha-1,3-galactosyltransferase knockout pigs by breeding and somatic cell nuclear transfer. Xenotransplantation 2007; 14: 339–344.
4. KUWAKI K, TSENG YL, DOR F et al. Heart transplantation in baboons using 1,3-galactosyl transferase gene-knockout pigs as donors: initial experience. Nat Med 2005; 11: 29–31.
5. YAMADA K, YAZAWA K, SHIMIZU A et al. Marked prolongation of porcine renal xenograft survival in baboons through the use of alpha 1,3-galactosyltransferase gene-knockout donors and the cotransplantation of vascularized thymic tissue. Nat Med 2005; 11: 32–34.
6. CHEN G, QIAN H, STARZ T et al. Acute rejection is associated with antibodies to non-Gal antigens in baboons using Gal-knockout pig kidneys. Nat Med 2005; 11: 1295–1298.
7. NGUYEN B-NH, AZIMZADEH AM, ZHANG T et al. Life-supporting function of genetically modified swine lungs in baboons. J Thorac Cardiovasc Surg 2007; 133: 1354–1363.
8. COOPER DKC, DORLING A, PIERSON RN et al. alpha 1,3-galactosyltransferase gene-knockout pigs for xenotransplantation: where do we go from here? Transplantation 2007; 84: 1–7.
9. YANG Y-G, SYKES M. Xenotransplantation: current status and a perspective on the future. Nat Rev Immunol 2007; 7: 519–531.
10. SACHS DH, SYKES M, YAMADA K. Achieving tolerance in pig-to-primate xenotransplantation: reality or fantasy. Transpl Immunol 2009; 21: 101–105.
11. PIERSON RN III. Antibody-mediated xenograft injury: mechanisms and protective strategies. Transpl Immunol 2009; 21: 65–69.
12. D'APICE AJF, COWAN PJ. Gene-modified pigs. Xenotransplantation 2008; 15: 87–90.
13. SPRANGERS B, WAER M, BILLIAU AD. Xenotransplantation: where are we in 2008? Kidney Int 2008; 74: 14–21.
14. COWAN PJ, AMINIAN A, BARLOW H et al. Renal xenografts from triple-transgenic pigs are not hyperacutely rejected but cause coagulopathy in non-immunosuppressed baboons. Transplantation 2000; 69: 2504–2515.
15. COZZI E, BHATTI F, SCHMOECKEL M et al. Long-term survival of nonhuman primates receiving life-supporting transgenic porcine kidney xenografts. Transplantation 2000; 70: 15–21.
16. HOUSER SL, KUWAKI K, KNOSALLA C et al. Thrombotic microangiopathy and graft arteriopathy in pig hearts following transplantation into baboons. Xenotransplantation 2004; 11: 416–425.
17. MCGREGOR CGA, DAVIES WR, OI K et al. Cardiac xenotransplantation: recent preclinical progress with 3-month median survival. J Thorac Cardiovasc Surg 2005; 130: 844–851.
18. COLVIN RB, SMITH RN. Antibody-mediated organ-allograft rejection. Nat Rev Immunol 2005; 5: 807–817.
19. RITTIRSCH D, FLIERL MA, WARD PA. Harmful molecular mechanisms in sepsis. Nat Rev Immunol 2008; 8: 776–787.
20. WASOWSKA BA, LEE CY, HALUSHKA MK, BALDWIN WM. New concepts of complement in allorecognition and graft rejection. Cell Immunol 2007; 248: 18–30.
21. BHATTI FNK, SCHMOECKEL M, ZAIDI A et al. Three-month survival of HDAFF transgenic pig hearts transplanted into primates. Transplant Proc 1999; 31: 958–958.
22. LIU DG, KOBAYASHI T, ONISHI A et al. Relation between human decay-accelerating factor (hDAF) expression in pig cells and inhibition of human serum anti-pig cytotoxicity: value of highly expressed hDAF for xenotransplantation. Xenotransplantation 2007; 14: 67–73.
23. OGAWA H, MURAMATSU H, KOBAYASHI T et al. Molecular cloning of endo-beta-galactosidase C and its application in removing alpha-galactosyl xenoantigen from blood vessels in the pig kidney. J Biol Chem 2000; 275: 19368–19374.
24. OGAWA H, KOBAYASHI T, YOKOYAMA I et al. Reduction of alpha-galactosyl xenoantigen by expression of endo-beta-galactosidase C in pig endothelial cells. Xenotransplantation 2002; 9: 290–296.
25. ONISHI A, IWAMOTO M, AKITA T et al. Pig cloning by microinjection of fetal fibroblast nuclei. Science 2000; 289: 1188–1190.
26. NIWA H, YAMAMURA K, MIYAZAKI J. Efficient selection for high-expression transfectants with a novel eukaryotic vector. Gene 1991; 108: 193–199.
27. LIU DG, KOBAYASHI T, YOKOYAMA I et al. Enzymatic removal of alpha Gal antigen in pig kidneys by ex vivo and in vivo administration of endo-beta-galactosidase C. Xenotransplantation 2002; 9: 228–236.
28. IWAMOTO M, ONISHI A, FUCHIMOTO D et al. Effects of caffeine treatment on aged porcine oocytes: parthenogenetic activation ability, chromosome condensation and development to the blastocyst stage after somatic cell nuclear transfer. Zygote 2005; 13: 335–345.
29. YOSHIOKA K, SUZUKI C, TANAKA A, ANAS IMK, IWAMURA S. Birth of piglets derived from porcine zygotes cultured in a chemically defined medium. Biol Reprod 2002; 66: 112–119.
30. WAKAYAMA T, PERRY ACF, ZUCCOTTI M, JOHNSON KR, YANAGIMACHI R. Full-term development of mice from enucleated oocytes injected with cumulus cell nuclei. Nature 1998; 394: 369–374.
31. KOBAYASHI T, YOKOYAMA I, MOROZUMI K et al. Comparative study of efficacy of removal of anti-ABO and anti-gal antibodies by double filtration plasmapheresis. Xenotransplantation 2000; 7: 101–108.
32. WATANABE S, IWAMOTO M, SUZUKI S et al. A novel method for the production of transgenic cloned pigs: electroporation-mediated gene transfer to non-cultured cells and subsequent selection with puromycin. Biol Reprod 2005; 72: 309–315.
33. KOBAYASHI T, LIU DG, MIWA Y et al. Immunogenicity of cloned pig cells expressing only 1% of alpha Gal antigens. Xenotransplantation 2005; 12: 375–375.
34. COSTA C, BROKAW JL, WANG Y, FODOR WL. Delayed rejection of porcine cartilage is averted by transgenic expression of alpha 1,2-fucosyltransferase. FASEB J 2003; 17: 109–111.
35. MIYAGAWA S, MURAKAMI H, TAKAHAGI Y et al. Remodeling of the major pig xenoantigen by N-acetylglucosaminyltransferase III in transgenic pig. J Biol Chem 2001; 276: 39310–39319.

Cardiovascular Research Advance Access published January 19, 2010

Cardiovascular Research
doi:10.1093/cvr/cvp386

Midkine gene transfer after myocardial infarction in rats prevents remodelling and ameliorates cardiac dysfunction

Arihiro Sumida[1†], Mitsuru Horiba[1*†], Hisaaki Ishiguro[1,2], Hiroharu Takenaka[1,3], Norihiro Ueda[1], Hiroaki Ooboshi[4], Tobias Opthof[5,6], Kenji Kadomatsu[7], and Itsuo Kodama[1]

[1]Department of Cardiovascular Research, Research Institute of Environmental Medicine, Nagoya University, Huro-cho, Chikusa-ku, Nagoya 464-8601, Japan; [2]Department of Cardiology, Nagoya University Graduate School of Medicine, Nagoya, Japan; [3]Department of Cardiothoracic Surgery, Nagoya University Graduate School of Medicine, Nagoya, Japan; [4]Department of Medicine and Clinical Science, Graduate School of Medical Sciences, Kyusyu University, Fukuoka, Japan; [5]Experimental Cardiology Group, Center for Heart Failure Research, Academic Medical Center, Amsterdam, the Netherlands; [6]Department of Medical Physiology, University Medical Center Utrecht, Utrecht, the Netherlands; and [7]Department of Biochemistry, Nagoya University Graduate School of Medicine, Nagoya, Japan

Received 16 February 2009; revised 30 October 2009; accepted 23 November 2009

Time for primary review: 36 days

Aim We have previously reported that therapy with midkine (MK) has a protective effect in mouse models of myocardial infarction (MI) and ischemia/reperfusion. The underlying mechanism was proved to be anti-apoptosis and prevention of left ventricular (LV) remodelling following angiogenesis. Here we investigated the effects of overexpression of MK by adenoviral gene transfer on cardiac function and remodelling in an experimental rat MI model.

Methods and results MI was created in male Wistar rats. Adenoviral vectors encoding mouse MK (AdMK) or β-galactosidase (AdLacZ; as controls) were injected in myocardium at the onset of MI. One week after injection, *in vivo* adenoviral gene expression was assessed by western blot and histological analysis. After echocardiographic analysis at 4 weeks and haemodynamic analysis at 6 weeks after MI, AdMK animals had better cardiac function compared with AdLacZ animals. Heart weight (HW) and relative HW of AdMK animals were not different from sham-operated animals after 6 weeks, pointing to a very potent effect in the prevention of ischemic cardiomyopathy. In histological studies at 6 weeks after MI, AdMK animals had less fibrosis in the non-infarcted myocardium and higher vascular density in the border-zone area compared with AdLacZ animals. AdMK animals had strongly upregulated levels of phosphorylated extracellular signal-regulated kinase, Akt, PI 3-kinase, and Bcl-2, whereas the level of Bax was downregulated compared with AdLacZ animals.

Conclusion Overexpression of MK prevents LV remodelling and ameliorates LV dysfunction by anti-apoptotic and pro-angiogenic effects. MK gene transfer may provide a new therapeutic modality in ischemic cardiomyopathy and ischemic heart failure.

Keywords Gene transfer • Coronary disease • Infarction • Haemodynamics • Remodelling

1. Introduction

Midkine (MK) is a heparin-binding growth factor involved in neural survival, carcinogenesis, and tissue repair.[1] The mobilization of inflammatory cells is closely related to the angiogenic efficacy of MK.[2] During embryogenesis, MK is highly expressed in the mid-gestational period and then decreases to birth. MK is expressed at the interface between mesenchyme and epithelium, and the expression is limited to adult organs where this interaction occurs/remains. Kidney and uterus are typical organs formed at

†These authors contributed equally to this work

* Corresponding author. Tel: +81 52 789 3871; fax: +81 52 789 3890, Email: mhoriba@riem.nagoya-u.ac.jp

the epithelial–mesenchymal interaction. In a normal heart, the expression of MK is very weak, thus MK is neither considered to be involved in normal cardiac development, nor does it affect normal cardiac function. Myocardial infarction (MI) strongly induces MK expression in the area adjacent to the infarction within 6 h after myocardial ischemia.[3] We previously showed that MK reduces apoptosis via extracellular signal-regulated kinase (ERK) phosphorylation and by Bcl-2 activation in mice subjected to ischemia/reperfusion.[4] In addition, we have recently reported that exogenous MK attenuates left ventricular (LV) remodelling and improves long-term survival after MI by enhancing angiogenesis and anti-apoptosis via the Akt/PI 3-kinase pathway.[5] Intramyocardial injection of collagen gel including MK also attenuates cardiac remodelling after MI by its angiogenetic action.[6] Adenoviral gene transfer has been applied in the treatment of ischemic myocardium in various experimental models.[7,8] Adenoviral gene transfer of MK had protective effects in a rat middle cerebral artery occlusion model and decreased brain infarct volume.[9] To date, it is unknown whether adenoviral vector transfer of MK has cardioprotective effects in myocardial ischemia. In the present study, we show that MK gene delivery is indeed effective in a rat MI model. In addition we have elucidated the underlying molecular biological mechanism.

2. Methods

2.1 Adenoviral vector construction

Replication-deficient (E1,E3 deleted) recombinant adenoviral vectors containing mouse MK transgene (AdMK) and β-galactosidase transgene (AdLacZ) as control vectors, driven by the cytomegalovirus, were used in the present study. These vectors were constructed at the University of Iowa Gene Transfer Vector Core (Beverly L. Davidson) and obtained via Kyusyu University (Tetsuro Ago).

2.2 Animal model

Male Wistar rats (8–10 weeks old, weight 222–325 g) were obtained from Chubu Kagaku Shizai. All animal experiments were performed in accordance with the *Guide for the Care and Use of Laboratory Animals* published by the US National Institutes of Health (NIH publication No. 85-23, revised 1996), and were approved by the Animal Care and Use Committee of Nagoya University. The rats were anaesthetized with intraperitoneal injection of pentobarbital sodium (50 mg/kg). After anaesthesia, the left coronary descending artery (LAD) was ligated to create a rat MI model. By electrocardiographic monitoring, a similar degree of ST elevation was observed in all MI rats. Then, they were randomly assigned to two groups. Thirty minutes after ligation, adenoviral vectors were injected intramyocardially with a 30-gauge needle. The control rats received injections of 1.0×10^9 plaque forming unit (PFU) of adenovirus encoding the β-galactosidase gene (AdLacZ) at five or six LV myocardial sites separated by 2 or 3 mm around the LAD. MK-treated rats were injected with 1.0×10^9 PFU of adenovirus encoding mouse MK gene (AdMK). A total of 250 μL of virus solution [3% sucrose in phosphate-buffered saline (PBS)] was injected, by a single investigator blinded to the types of adenoviral genes. After injection, air was evacuated from the cavity, and the chest was closed. Normal respiration was restored. Animals were housed in a temperature-controlled conventional facility (28°C) with free access to regular chow and water. They were euthanized at 1 or 6 weeks after MI.

Full details of these procedures are given in the Supplementary material online.

2.3 Echocardiography

Transthoracic echocardiography was performed to study cardiac functional parameters with a Nemio 20 (Toshiba Medical) before and after MI as described previously.[4] Each rat was anaesthetized with intraperitoneal injection of ketamine 50 mg/kg and xylazine 10 mg/kg. A single investigator blinded to the treatment groups performed all measurements.

Full details of these procedures are given in the Supplementary material online.

2.4 Cardiac haemodynamics

Cardiac haemodynamics were measured with a 1.4 F micro-tipped catheter (Millar instruments). The rats were anaesthetized as for echocardiography (see above). Full details of these procedures are given in the Supplementary material online. Thereafter, the rats were euthanized by injection of 1 mL of KCl (1 mEq/mL) into the LV cavity to arrest the heart in diastole. The heart was harvested and stored for histological, morphological, and molecular biological analyses.

2.5 X-gal staining

Hearts were fixed in 4% paraformaldehyde in PBS for 2 h, 20% sucrose in PBS at 4°C overnight, 30% sucrose in PBS for 2 h, and sliced and embedded in optimal cutting temperature compound to freeze with liquid nitrogen. For X-gal staining, frozen sections (8-μm thick) perpendicular to the apex-base axis of the LV were made with a cryostat and stained with X-gal solution as previously described.[10] The sections were rinsed in PBS and counterstained with neutral red before mounting. Full details of these procedures are given in the Supplementary material online.

2.6 Picrosirius red staining

After fixation with 4% paraformaldehyde in PBS, the hearts were sliced, embedded in paraffin and cut transversely into 6-μm thick sections. In addition to regular haematoxylin and eosin staining, the sections were stained with picrosirius red to analyse types I and III collagen accumulation as previously described.[10] Collagen deposition in the infarcted and non-infarcted areas was calculated as the percentage of stained tissue in the summed area of muscular and connective tissue by densitometry using Scion Image 4.0.3 (Scion Corporation). Full details of these procedures are given in the Supplementary material online.

2.7 Immunohistochemistry

Paraffin sections (thickness 6 μm) were processed for the von Willebrand factor (vWf) immunohistochemical staining after having been deparaffinized. Antigen was retrieved as previously described.[11] To detect microvascular density in the peri-infarct area, a rabbit anti-vWf antibody was used as a primary antibody. Secondary antibodies were biotinylated using goat anti-rabbit IgG and a streptavidin-horseradish peroxidase (Blood Vessel Staining Kit, CHEMICON). Subsequently, the relevant antigen was visualized using an avidin–biotin peroxidase complex and 3,3′-diamino-benzidine tetrahydrochloride. Nuclei were stained with haematoxylin. The number of capillary vessels in the border-zone area was counted using light microscopy (Microphot-FXA, Nicon) by a blinded investigator in 10 randomly selected areas and subsequently averaged.

2.8 Western blotting analysis

Levels of MK, ERK-1/2, Akt, PI 3-kinase, Bcl-2, and Bax proteins in the border-zone of LV myocardium were assessed by western blots at 1 week after MI as previously described.[4] Briefly, LV myocardial homogenates were subjected to sodium dodecyl sulphate-polyacrylamide gel electrophoresis on a 10–12.5% polyacrylamide gel and proteins were electroblotted on the membranes (Atto). After blocking for 1 h, the membranes were incubated with primary and secondary antibodies in PBS-T or TBS-T solutions for 1 h each. Antibodies against MK,[4] phospho-Akt/PKBα (Upstate), Akt/PKBα (Upstate), diphospho-ERK-1/2 (Sigma), ERK1/2 (Sigma), anti-PI3K (Upstate), Bax (Santa Cruz), and Bcl-2 (Santa Cruz) were used as primary antibodies, respectively. Horseradish peroxidase-conjugated goat anti-rabbit immunoglobulin G (Sigma) and horseradish peroxidase-conjugated goat anti-mouse immunoglobulin G (Jackson Immunoresearch) were used as secondary antibodies. Dynabeads Protein G (Dynal Biotech) was used for immunoprecipitation (IP). ECL Plus Detection Reagents (GE Healthcare) were used as enhancers and for band detection of each protein, CoolSaver 1.0 (Atto) was used. The intensity of bands was quantified by densitometry with CS analyser 3.0 (Atto).

2.9 Statistical analysis

Data analyses were performed with SPSS for Windows (version 16.0). All data were described as mean ± SEM. Comparisons between two groups were analysed using Student's *t*-test. Statistical comparisons among the groups were performed by ANOVA with Bonferroni post-hoc tests. A value of $P < 0.05$ was considered as statistically significant.

3. Results

MI was made in 30 rats. One rat had died before adenoviral injection. Of the 29 rats, 15 rats were injected with AdLacZ and 14 with AdMK. Three of the 15 AdLacZ rats had died before echocardiography at 4 weeks after MI. Two of 14 AdMK rats had died before echocardiography. Therefore, both the AdLacZ MI group and the AdMK MI group consisted of 12 animals. All five rats which had died before analyses had a large amount of pleural effusion due to heart failure. Sham-operated 8 rats (without MI: sham) all survived. Thus, there were three groups of rats. Group 1 consisted of these eight sham-operated rats that were either injected with AdLacZ (sham + AdLacZ, $n = 4$) or AdMK (sham + AdMK, $n = 4$). Group 2 comprised rats that were injected with AdLacZ 30 min after occlusion of the LAD (the AdLacZ group, $n = 12$) and group 3 consisted of rats injected with AdMK 30 min after occlusion (the AdMK group, $n = 12$).

3.1 Adenoviral gene expression after intramyocardial injection

To confirm adenoviral infection and gene expression, control rats were sham operated. AdLacZ or AdMK rats were injected into the LV myocardium around the LAD. One week after injection, the rats were sacrificed to estimate adenoviral gene transfer. Cells were stained blue after X-gal staining at the injected sites of the LV in the AdLacZ group, indicating expression of the β-galactosidase gene (*Figure 1A*, red arrows). They were seen throughout the injected areas of the rat LV wall. In western blotting followed by IP with proteins from ventricular homogenates, the LV myocardium of the AdMK group showed substantial overexpression of MK protein as strong as in the kidney, which possesses abundant endogenous MK protein. In contrast, the expression of MK protein was not detected in the AdLacZ group (*Figure 1B*). Thus AdLacZ and AdMK were successfully injected into the LV myocardium. In addition, the transferred adenoviral genes were effectively expressed in *in vivo* rat hearts. To examine the long-term MK expression by adenoviral gene transfer, we also analysed the expression of MK at 1, 2, 4, 6, 8, and 10 weeks after gene transfer in sham-operated rats by western blots. *Figure 1C* shows the time course of MK expression after AdMK injection. The expression of MK declined gradually

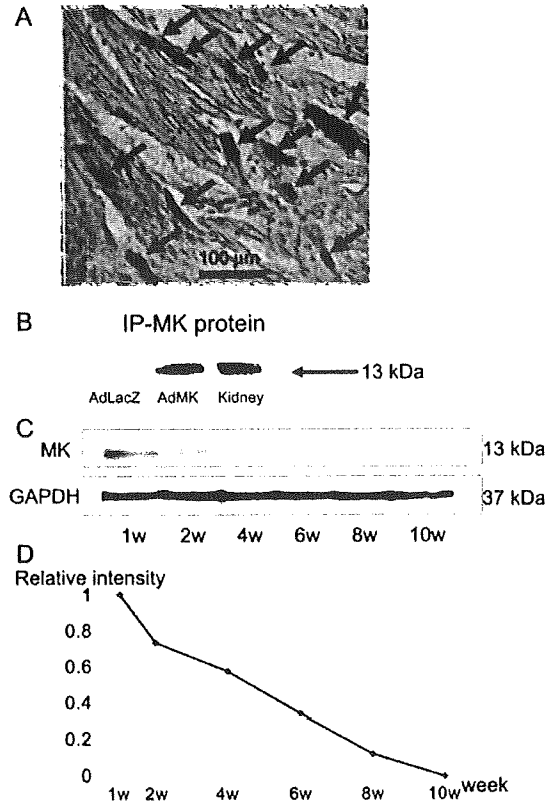

Figure 1 *In vivo* adenoviral infection and gene expression at 1 week after injection into LV myocardium of rat heart without MI. (*A*) Representative X-gal staining with counterstaining neutral red of heart section in the AdLacZ group. Red arrows point to the cells stained blue which express β-galactosidase gene in the injected LV myocardium. Scale bar represents 100 μm. (*B*) Immuno-blots with IP for MK protein (13 kDa) were performed by using ventricular homogenates in the injected areas with AdLacZ or AdMK and kidney homogenates. (*C*) Western blot of MK protein was performed by using the injected myocardium in sham-operated rats. Representative bands of MK and GAPDH at 1, 2, 4, 6, 8, 10 weeks after AdMK injection are demonstrated. (*D*) The graph shows the expressions of MK at each week. They were represented with relative intensity to 1 week.

Table 1 Echocardiographic data at 4 weeks after MI

	Sham-operated rats (n = 8)			AdLacZ rats (n = 12)	AdMK rats (n = 12)
	Sham + AdLacZ (n = 4)	Sham + AdMK (n = 4)			
HR, b.p.m	276 ± 17	280 ± 22	278 ± 19	279 ± 28	281 ± 35
LVEF, %	73.5 ± 4.4	75.0 ± 3.7	74.3 ± 3.9	29.5 ± 4.4*	51.3 ± 5.0***
FS, %	37.5 ± 3.7	39.3 ± 3.4	38.4 ± 3.4	12.4 ± 2.1*	23.0 ± 2.8***
LVEDD, mm	6.9 ± 0.4	7.1 ± 0.8	7.0 ± 0.6	10.7 ± 0.7*	8.7 ± 0.7***
LVESD, mm	4.2 ± 0.3	4.2 ± 0.5	4.2 ± 0.4	9.3 ± 0.7*	6.7 ± 0.7***
BWT, mm	1.3 ± 0.4	1.4 ± 0.1	1.3 ± 0.3	0.6 ± 0.1*	0.9 ± 0.2***

Sham + AdLacZ means sham-operated rats injected with AdLacZ. Sham + AdMK means sham-operated rats injected with AdMK. LVEF, left ventricular ejection fraction; FS, fractional shortening; LVEDD, left ventricular end-diastolic dimension; LVESD, left ventricular end-systolic dimension; BWT, border-zone wall thickness. LVEF = $[(LVEDD^3 - LVESD^3)/LVEDD^3] \times 100$ and FS = (LVEDD − LVESD)/LVEDD × 100. Values are mean ± SEM.
*$P < 0.001$ vs. sham-operated rats.
**$P < 0.001$ vs. AdLacZ rats.

from 1 week on. It was weakly detectable at 8 weeks and it was no longer detectable at 10 weeks after adenoviral injection (*Figure 1D*).

3.2 Prevention of LV remodelling and amelioration of dysfunction after MI

There were no pre-operative differences among groups 1–3 before MI with left ventricular ejection fraction (LVEF) of 78.9 ± 7.3%. Echocardiography was repeated at 4 weeks after MI. There were no differences in any parameters between the two sham subgroups (sham + AdLacZ group and sham + AdMK group; *Table 1*). At 4 weeks after MI, the AdMK treated rats showed a smaller LV cavity and better contractile function compared with the AdLacZ rats (*Figure 2A* and *B*). LVEF and fractional shortening were significantly higher in the AdMK group compared with those in the AdLacZ group (*Table 1*). In addition, left ventricular end-diastolic dimension (LVEDD) and left ventricular end-systolic dimension (LVESD) were significantly smaller compared with the AdLacZ group. The border-zone wall thickness (BWT) was larger in the AdMK group compared with the AdLacZ group. All parameters in the AdMK group were in-between those in the sham and AdLacZ groups (*Table 1*). Also, all differences among the three groups were significant except heart rate (*Table 1*). AdMK significantly mitigates all pathophysiological contractile changes caused by MI.

3.3 Haemodynamics and morphological analysis

Haemodynamic data were obtained at 6 weeks after MI by LV catheterization to assess the LV function and the degree of heart failure. There were no differences in any parameters between the two sham subgroups (sham + AdLacZ group and sham + AdMK group; *Table 2*). The AdMK group had higher maximum dP/dt (dP/dt_{max}) and lower minimum dP/dt ($-dP/dt_{min}$) compared with the AdLacZ group (*Table 2*). The AdMK group also had lower LVEDP compared with the AdLacZ group. The dP/dt_{max}, $-dP/dt_{min}$, and LVEDP values in the AdMK group were in-between those in the sham and AdLacZ groups (*Table 2*). Also, all differences between the three groups were significant (*Table 2*).

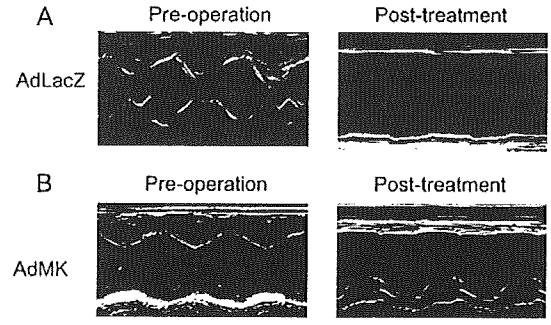

Figure 2 Echocardiography prior to and 4 weeks after MI. (*A*) Representative M-mode findings in the AdLacZ group before MI (pre-operation) and 4 weeks after MI (post-treatment). (*B*) Representative M-mode findings in the AdMK group before MI (pre-operation) and 4 weeks after MI (post-treatment).

In fact, from the almost three-fold increase in LVEDP caused by MI (from 2.1 mmHg in sham to 8.3 mmHg in AdLacZ group), only 16% remained in the AdMK group (*Table 2*). After AdMK injection, heart weight (HW) and heart weight/body weight (HW/BW) ratio were significantly lower than in the AdLacZ group, whereas the difference with the sham-operated group was insignificant, underscoring the high efficacy of MK against the development of ischemic cardiomyopathy.

3.4 Reduction of collagen deposition after MI

Picrosirius red staining was performed at 6 weeks after MI to visualize types I and III collagen deposition in LV cross-sections. *Figure 3A* shows collagen deposition in red and normal myocardium in yellow in a representative AdLacZ heart with MI. *Figure 3B* shows prominent reduction of collagen deposition in the non-infarcted myocardium in a heart from the AdMK group compared with the AdLacZ group (*Figure 3A*). Also the infarct itself was much smaller (compare *Figure 3B* with *A*). At the border-zone area of the

Table 2 Haemodynamic and morphological data at 6 weeks after MI

	Sham-operated rats (n = 8)		AdLacZ rats (n = 12)	AdMK rats (n = 12)
	Sham + AdLacZ (n = 4)	Sham + AdMK (n = 4)		
HR, b.p.m	266 ± 26	255 ± 13	261 ± 20	266 ± 18	263 ± 21
LVEDP, mmHg	2.1 ± 0.1	2.1 ± 0.2	2.1 ± 0.2	8.3 ± 2.2*	3.1 ± 0.8**,****
dP/dt_{max}, mmHg/s	5802 ± 248	5790 ± 306	5796 ± 258	2171 ± 763*	3217 ± 522**,****
$-dP/dt_{min}$, mmHg/s	−5737 ± 757	−5764 ± 470	−5751 ± 584	−1700 ± 722*	−2650 ± 824**,****
BW, g (pre-operation)	276 ± 13	280 ± 15	278 ± 13	276 ± 35	270 ± 21
BW, g (post-treatment)	385 ± 16	391 ± 26	388 ± 20	390 ± 34	399 ± 22
HW, mg	1201 ± 127	1196 ± 98	1198 ± 105	1561 ± 181*	1245 ± 98***
HW/BW, mg/g	3.11 ± 0.24	3.07 ± 0.17	3.09 ± 0.19	4.04 ± 0.67*	3.13 ± 0.31***

Sham + AdLacZ and sham + AdMK are used as the same in *Table 1*. HR, heart rate; LVEDP, left ventricular end-diastolic pressure; dP/dt_{max} and $-dP/dt_{min}$, maximal and minimal first derivatives of LV pressure; BW, body weight; HW, heart weight. Values are mean ± SEM.
*$P < 0.001$ vs. sham-operated rats.
**$P < 0.01$ vs. sham-operated rats.
***$P < 0.001$ vs. AdLacZ rats.
****$P < 0.01$ vs. AdLacZ rats.

infarct LV myocardium, the AdMK group had a higher density of collagen deposition and a thicker fibrotic wall (*Figure 3D*) compared with the AdLacZ group (*Figure 3C*). In contrast, the AdMK group had less fibrosis in the non-infarct area (*Figure 3F*) compared with the AdLacZ group (*Figure 3E*). *Figure 3G* shows a quantification of areas of collagen deposition in the non-infarct areas in the hearts from the AdLacZ and AdMK groups. In the AdMK group, there was a reduction of more than 50% of collagen deposition compared with the AdLacZ group.

3.5 Enhancement of neovascularization

To quantify neovascularization in the peri-infarct area of the rat heart, vWf immunohistochemical staining was carried out at 6 weeks after MI. *Figure 4A* shows vWf positive staining (dark brown) in capillary vessels (red arrows) in the peri-infarct area of representative samples from the AdLacZ, AdMK, and control group. Control sections refer to sections from AdMK hearts stained without the primary antibody. Negative staining in these controls indicate that the immunostaining was specific (*Figure 4A*). The AdMK group had a 50% higher vWf positive capillary density in the peri-infarct area compared with the AdLacZ group (*Figure 4B*). Thus, AdMK enhances angiogenesis in the peri-infarct area after MI.

3.6 Upregulation of PI3k/Akt and ERK pathways

One week after MI, border-zone myocardium was collected for western blot analysis. To elucidate the mechanism of angiogenesis, phosphorylation of Akt and ERK-1/2 and PI 3-kinase protein levels were evaluated by densitometry of western blotting. *Figure 5A* shows the substantially higher intensity of phosphorylated Akt (phospho-Akt), phosphorylated ERK-1/2 (phospho-ERK-1/2), and PI 3-kinase in the AdMK group compared with the AdLacZ group while total Akt, total ERK-1/2, and GAPDH showed similar expression in both groups. For phosphorylated Akt, phosphorylated ERK-1/2, and PI 3-kinase, the levels were increased by 77, 43, and 136%, respectively, in the AdMK group compared with the AdLacZ group (*Figure 5B*). AdMK enhances angiogenesis (*Figure 4*), and this angiogenetic action may thus be mediated by PI3K/Akt and ERK-1/2 pathways (*Figure 5B*).

3.7 Anti-apoptotic effects of the Bcl-2 family

To elucidate the mechanism of anti-apoptosis, Bcl-2 and Bax protein levels were evaluated by western blots as described in the previous section. *Figure 6A* shows representative bands of increased Bcl-2 and decreased Bax proteins in the AdMK group compared with the AdLacZ group with similar expression of GAPDH in both groups. *Figure 6B* shows the quantified changes with doubling of Bcl-2 protein and a four-fold reduction of the Bax protein in the AdMK group. AdMK may promote anti-apoptosis in the heart after MI by upregulating the anti-apoptotic Bcl-2 protein and by downregulating the pro-apoptotic Bax protein.

4. Discussion

In this study, we have presented long-term effects of MK gene transfer in a setting of chronic MI. As a result from infarct reduction, LVEDD and LVESD in the AdMK group were smaller than those in the AdLacZ group, and the larger BWT in the AdMK group limited the deterioration of LVEF and SF after MI. Mitigation of ischemic cardiomyopathy by AdMK treatment normalized the HW/BW ratio after MI compared with the AdLacZ group to values not different from sham-operated animals. Haemodynamically, systolic and diastolic functions in the AdMK group were better than in the AdLacZ group, although still worse than in sham-operated animals. Nevertheless, most parameters in the AdMK group were much closer to those in the sham group without MI than to those in the AdLacZ group with MI.

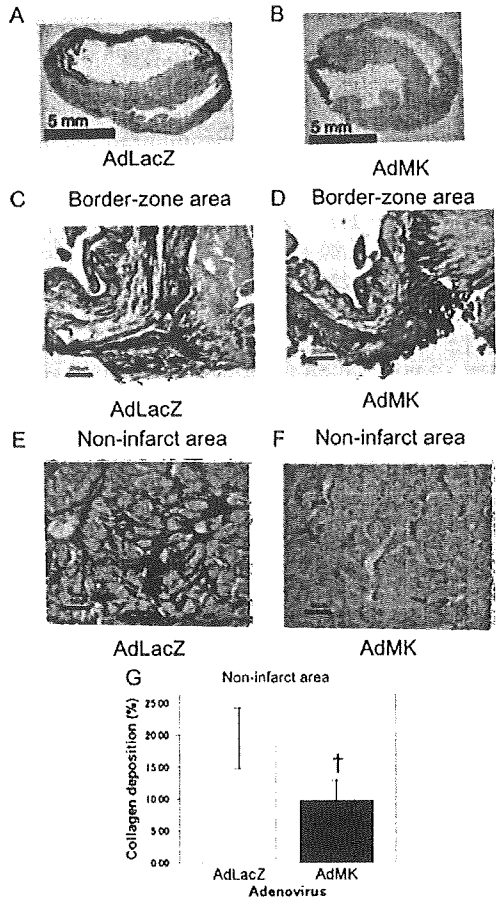

Figure 3 Picrosirius red staining at 6 weeks after MI to quantify collagen deposition. (*A*) Representative cross-section of an infarcted heart from the AdLacZ group. (*B*) Representative cross-section of an infarcted heart from the AdMK group. Scale bars represent 5 mm. (*C*) Representative border-zone area of infarcted heart from the AdLacZ group. (*D*) Representative border-zone area of infarcted heart from the AdMK group. Scale bars represent 200 μm. (*E*) Representative non-infarct area of an MI heart from the AdLacZ group. (*F*) Representative non-infarct area of an MI heart from the AdMK group. Scale bars represent 50 μm. (*G*) Collagen deposition (%) in the non-infarct areas from the AdLacZ and AdMK groups. Values are mean ± SEM. $^{\dagger}P < 0.01$ vs. AdLacZ ($n = 12$ per each).

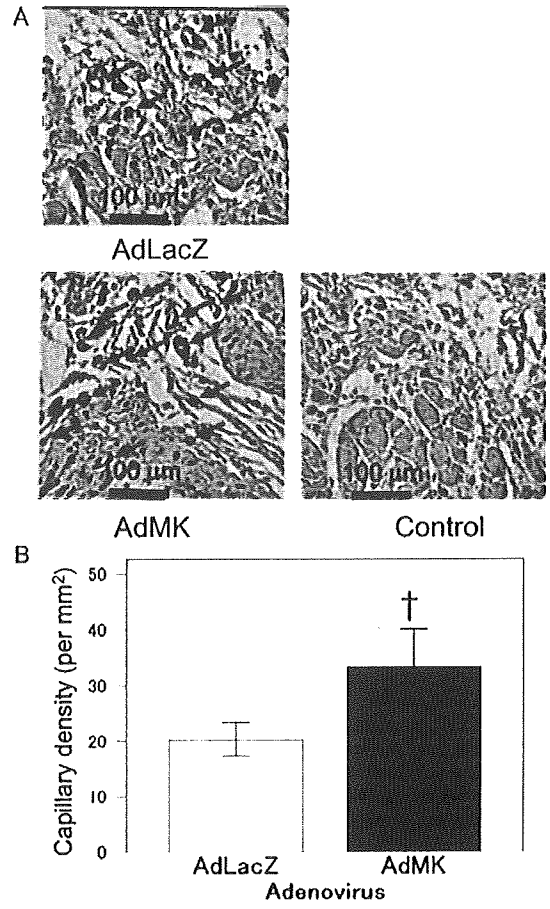

Figure 4 Immunohistochemical analyses for the von Willebrand factor (vWf) to quantify capillary vessels in the peri-infarct areas at 6 weeks after MI. (*A*) Cross-sections of representative peri-infarct areas from the AdLacZ, AdMK, and control group. The control group refers to sections from AdMK hearts stained without the primary antibody as a negative control for vWf staining. The vWf positive capillary vessels (red arrows) had tube formations and were stained dark brown with DAB (3,3′-diamino-benzidine tetrahydrochloride) substrates. Scale bar represents 100 μm. (*B*) The bar graphs represent the number of capillary vessels per 1 mm^2 of peri-infarct areas in the two groups. Values are mean ± SEM. $^{\dagger}P < 0.01$ vs. AdLacZ ($n = 12$ per each).

4.1 Adenoviral gene transfer of MK

Adenoviral gene transfer with intracoronary or intramyocardial injections has been used safely in clinical trials.[12–16] Local gene transfer of adenoviral vectors has some advantages in terms of the duration of the effects, the avoidance of systemic exposure, and the simplicity of delivery to target tissues compared with protein delivery. Different from other growth factors, gene therapy with overexpressed MK has never been reported previously. In this study, we have shown that adenoviral gene transfer of MK has strong effects on the infarcted heart comparable to previously reported MK protein therapy.[5,6]

4.2 Temporal aspects of adenoviral gene transfer of MK

In MI rats, cardiac dysfunction and chamber dilatation develop within 1 week after MI, and significant and rapid progressive LV dysfunction follows between the first and second month.[17] In addition, infarct expansion occurs within hours of myocyte injury, leading to wall thinning and ventricular dilatation and elevation of diastolic and systolic wall stress.[18] Infarct expansion also causes the deformation of the border-zone and remote normal myocardium, which alters the normal Frank–Starling relationship. The BWT was larger in the AdMK group compared

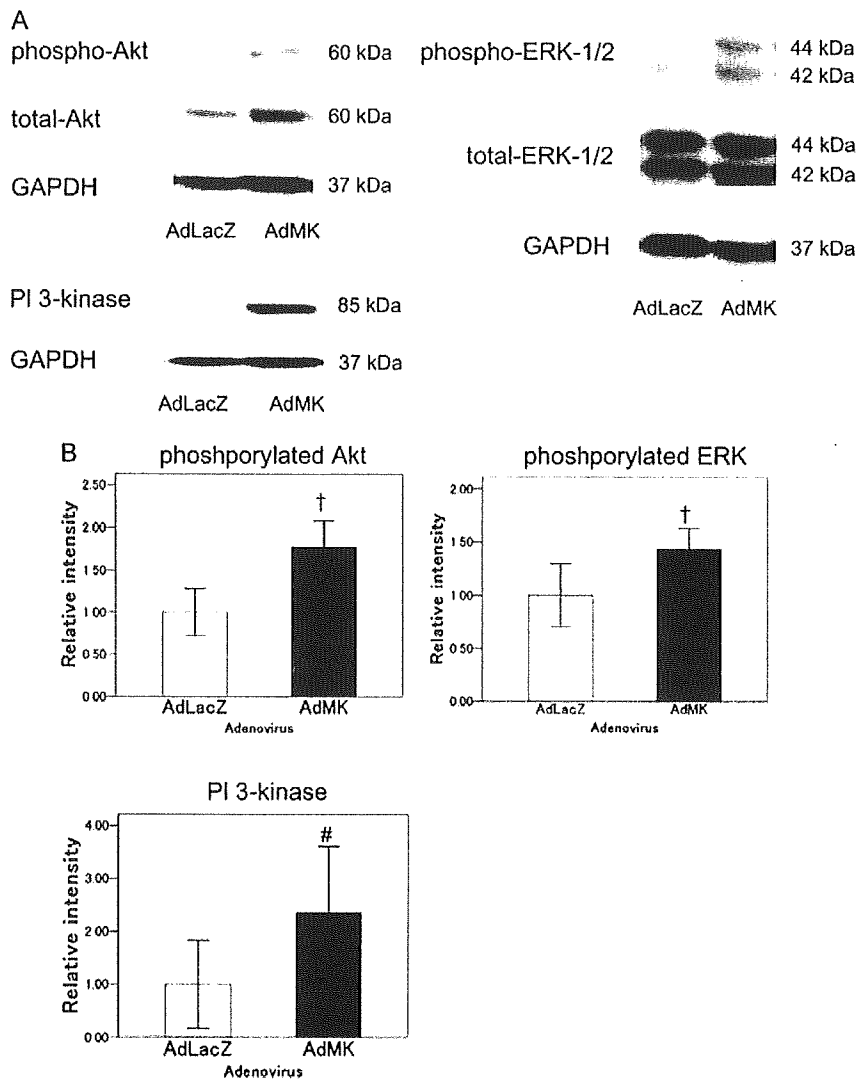

Figure 5 Western blotting analyses of Akt, ERK-1/2, PI 3-kinase protein were performed by using border-zone myocardium at 1 week after MI. (*A*) Representative bands of phosphorylated Akt, total Akt, phosphorylated ERK-1/2, total ERK-1/2, PI 3-kinase, and GAPDH are demonstrated. (*B*) The bar graphs of phosphorylated Akt and ERK show the ratio of the phosphorylated form of Akt or ERK to total Akt or ERK as relative intensity of the AdMK group compared with the AdLacZ group. The bar graphs of PI 3-kinase represents the relative intensity in the AdMK group compared with the AdLacZ group. Values are mean ± SEM. $^{\#}P < 0.05$, $^{\dagger}P < 0.01$ vs. AdLacZ ($n = 5$ per each).

with the AdLacZ group. This is consistent with improved cardiomyocyte survival promoted by increased Bcl-2 and decreased Bax activity and may constitute the key factor by which AdMK ameliorates cardiac dysfunction after MI. Adenovirus encoding MK apparently worked for at least 8 weeks after injection in the infarcted heart in order to explain the significant amelioration of LV dysfunction and remodelling at 4 weeks and even more obvious at 6 weeks after MI.

4.3 Reduction of fibrosis

Deposition of types I and III collagen occurs in infarcted and non-infarcted myocardium when intercellular signalling is potentiated by extensive myocardial necrosis.[18] MK has been reported to upregulate the expression of transforming growth factor-β_1 and to stimulate collagen production.[6,19,20] The border-zone wall composed of this thick fibrosis and the residual myocardium through anti-apoptosis in the AdMK group may retain LV geometry after MI. Thus AdMK may be correlated with the attenuation of tissue deformation in the non-infarct area and the prevention of collagen deposition in this area. Increased myocardial fibrosis directly links to abnormalities in diastolic function and myocardial stiffness.[21] In our study, collagen deposition in non-infarct area was reduced in the AdMK group compared with the AdLacZ group. The reduction of collagen deposition in non-infarcted myocardium in the AdMK group may result in the preservation of LV diastolic dysfunction after MI.

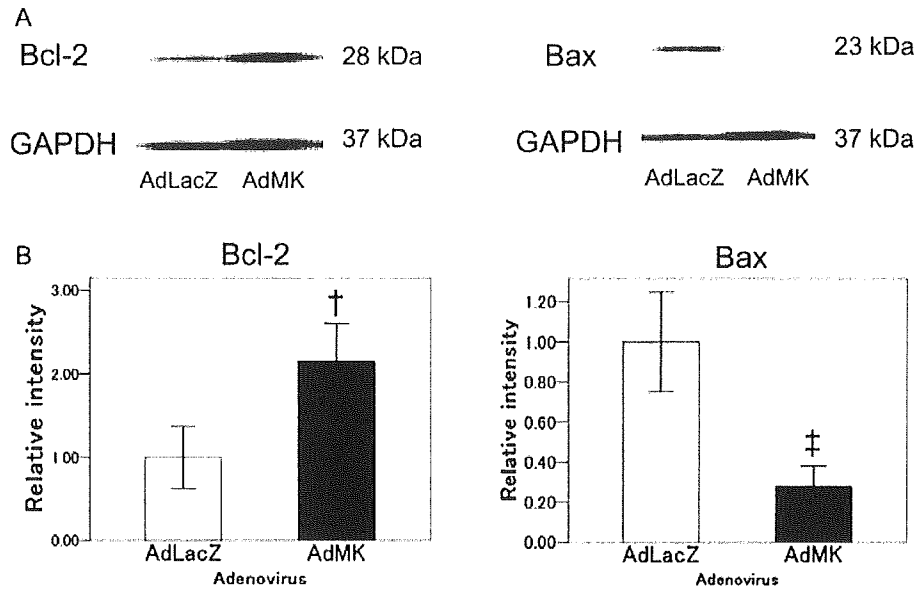

Figure 6 Western blotting analyses of Bcl-2 and Bax protein were performed by using border-zone myocardium at 1 week after MI. (*A*) Representative bands of Bcl-2, Bax, and GAPDH are shown. (*B*) The bar graphs of Bcl-2 and Bax represent the relative intensity in the AdMK group compared with the AdLacZ group. Values are mean ± SEM. $^{\dagger}P < 0.01$ vs. AdLacZ, $^{\ddagger}P < 0.001$ vs. AdLacZ ($n = 5$ per each).

4.4 Stimulation of angiogenesis and anti-apoptosis

MK has been reported to enhance tumour growth, endothelial cell proliferation, and vascular density. MK expression leads to the release of endothelial growth-stimulating factors from transfected cells, which confers an angiogenic activity on these cells, and this angiogenesis enhances both tumour growth and vascular density.[22] Collagen gel including MK enhances neovascularization in the infarct and border-zone area after MI.[6] MK also has anti-apoptotic effects via the activation of ERK, and MK also upregulates an anti-apoptotic factor, Bcl-2 in tumour cell lines and in cultured cardiomyocytes.[4,23,24] The enhancement of neovascularization and anti-apoptosis in the heart after MI by MK gene transfer may ameliorate cardiac dysfunction and prevent remodelling. Angiogenesis is particularly effective in the early post-infarction period when significant areas of border-zone myocardium are viable but hypokinetic or akinetic because of coronary ischemia. Also in the late remodelling phase neovascularization may permit collateral flow and attenuate the progression of late remodelling.[18] Correspondingly, the blockade of the activation of apoptosis following myocardial injury prevents cell loss and preserves myocardial geometry and function.[25,26]

4.5 Molecular mechanisms

In the present study, we elucidate the molecular biological background of angiogenetic and anti-apoptotic effects of MK gene transfer. The PI 3-kinase/Akt signalling pathway has a potential role in inhibition of cardiomyocyte apoptosis and induces vascularization of myocardium after MI.[27,28] The ERK-1/2 MAP kinase pathway is also a key signalling cascade in the modulation of angiogenesis and p38 MAPK/ERK-1/2 signalling is cardioprotective by suppression of apoptosis.[29,30] In the Bcl-2 family, the balance in expression between Bcl-2 and Bax has been suggested to be pivotal for apoptotic cell death.[31,32] In the AdMK group, the levels of phospho-Akt, phospho-ERK, and PI 3-kinase were significantly elevated compared with the AdLacZ group. Upregulation of Bcl-2 and downregulation of Bax shifted another anti-apoptotic balance in a favourable direction in the AdMK group.

4.6 Limitation and future aspects

MK promotes tumour angiogenesis as well as ischemic myocardial angiogenesis. Transient local administration, rather than systemic administration, may therefore limit the risk of carcinogenesis. But the application of angiogenic factors for the treatment of ischemic heart disease needs further thorough consideration of risk/benefit balance, in particular, in patients with carcinomas. In addition, adenovirus provokes an immune response and a significant inflammatory response apart from the induction of apoptosis.[8,33] Adenoviral vectors themselves should be improved for the purpose of delivering genes safely by percutaneous catheter-based myocardial injection or intracoronary injection.

In conclusion, we have demonstrated in this study that overexpression of MK improves long-term LV dysfunction and limits remodelling after MI through angiogenic and anti-apoptotic effects. MK gene therapy may have the potential of becoming a therapeutic strategy in ischemic heart disease and ischemic heart failure in the near future.

Supplementary material

Supplementary material is available at *Cardiovascular Research* online.

Acknowledgement

We thank T. Koike and M. Hojo for technical assistance.

Conflict of interest: none declared.

Funding

This work was supported by the Ministry of Education, Culture, Sports, Sciences and Technology, Japan.

References

1. Kadomatsu K, Muramatsu T. Midkine and pleiotrophin in neural development and cancer. *Cancer Lett.* 2004;**204**:127–143.
2. Horiba M, Kadomatsu K, Nakamura E, Muramatsu H, Ikematsu S, Sakuma S *et al.* Neointima formation in a restenosis model is suppressed in midkine-deficient mice. *J Clin Invest* 2000;**87**:489–495.
3. Obama H, Biro S, Ozawa M, Yoshida H, Tanaka H, Muramatsu T *et al.* Myocardial infarction induces expression of midkine, a heparin-binding growth factor with reparative activity. *Anticancer Res* 1998;**18**:145–152.
4. Horiba M, Kadomatsu K, Yasui K, Lee J-K, Muramatsu T, Kodama I *et al.* Midkine plays a protective role against cardiac ischemia/reperfusion injury through a reduction of apoptotic reaction. *Circulation* 2006;**114**:1713–1720.
5. Takenaka H, Horiba M, Sumida A, Ueda Y, Kodama I, Kadomatsu K *et al.* Midkine prevents ventricular remodeling and improves long-term survival after myocardial infarction. *Am J Physiol Heart Circ Physiol* 2009;**296**:H462–H469.
6. Fukui S, Kitagawa-Sakakida S, Matsumiya G, Kawaguchi N, Matsuura N, Sawa Y *et al.* Therapeutic effect of midkine on cardiac remodeling in infarcted rat heart. *Ann Thorac Surg* 2008;**85**:562–570.
7. Yu Y, Zhang Z-H, Wei S-G, Chu Y, Weiss RM, Heistad D *et al.* Central gene transfer of interleukin-10 reduces hypothalamic inflammation and evidence of heart failure in rats after myocardial infarction. *Circ Res* 2007;**101**:304–312.
8. Hao X, Masson-Broberg A, Grinnemo K-H, Siddiqui AJ, Dellgren G, Brodin LA *et al.* Myocardial angiogenesis after plasmid or adenoviral VEGF-A_{165} gene transfer in rat myocardial infarction model. *Cardiovasc Res* 2007;**73**:481–487.
9. Takada J, Ooboshi H, Kadomatsu K, Muramatsu T, Ibayshi S, Iida M *et al.* Postischemic gene transfer of midkine, a neurotrophic factor, protects against focal brain ischemia. *Gene Ther.* 2005;**12**:487–493.
10. Shinohara M, Hirata K, Emoto N, Inoue N, Yokoyama M, Kawashima S *et al.* Local overexpression of toll-like receptors at the vessel wall induces atherosclerotic lesion formation: synergism of TLR2 and TLR4. *Arterioscler Thromb Vasc Biol* 2007;**27**:2384–2391.
11. Kanellakis P, Slater NJ, Du X-J, Bobik A, Curtis DJ. Granulocyte colony-stimulating factor and stem cell factor improve endogenous repair after myocardial infarction. *Cardiovasc Res* 2005;**70**:117–125.
12. Giordano FJ, Ping P, Demaria AN, Dillmann WH, Mathieu CO, Hammond HK *et al.* Intracoronary gene transfer of fibroblast growth factor-5 increases blood flow and contractile function in an ischemic region of the heart. *Nat. Med* 1996;**2**:534–539.
13. Grines CL, Watkins MW, Rade JJ, Marrott P, Kirk HH, Engler RL *et al.* Angiogenic gene therapy (AGENT) trial in patients with stable angina pectoris. *Circulation* 2002;**105**:1291–1297.
14. Posengart TK, Lee LY, Grasso TM, Lesser ML, Isom W, Crystal RG *et al.* Angiogenesis gene therapy: phase I assessment of direct intramyocardial administration of an adenovirus vector expressing VEGF121 cDNA to individuals with clinically significant severe coronary artery disease. *Circulation* 1999;**100**:468–474.
15. Losordo DW, Vale PR, Hendel RC, Asahara T, Isner JM, Kunts RE *et al.* Phase 1/2 placebo-controlled, double-blind, dose-escalating trial of myocardial vascular endothelial growth factor 2 gene transfer by catheter delivery in patients with chronic myocardial ischemia. *Circulation* 2002;**105**:2012–2018.
16. Gyongyosi M, Khorsand A, Sochor H, Maurer G, Glogar D, Sylven C *et al.* NOGA-guided analysis of regional myocardial perfusion abnormalities treated with intramyocardial injections of plasmid encoding vascular endothelial growth factor A-165 in patients with chronic myocardial ischemia: subanalysis of EUROINJECT-ONE multicenter double-blind randomized study. *Circulation* 2005;**112**:157–165.
17. Liu Y-H, Yang X-P, Nass O, Sabbah HN, Peterson E, Carretero OA. Chronic heart failure induced by coronary artery ligation in Lewis inbred rats. *Am J Physiol* 1997;**272**:H722–H727.
18. Sutton MG, Sharpe N. Left ventricular remodeling after myocardial infarction: Pathophysiology and therapy. *Circulation* 2000;**101**:2981–2988.
19. Yamada H, Inazumi T, Tajima S, Muramatsu H, Muramatsu T. Stimulation of collagen expression and glycosaminoglycan synthesis by midkine in human skin fibroblast. *Arch Dermatol Res* 1997;**289**:423–433.
20. Sato W, Kadomatsu K, Yuzawa Y, Muramatsu H, Hotta N, Matsuo S *et al.* Midkine is involved in neutrophil infiltration into the tubulointerstitium in ischemic renal injury. *J Immunol* 2001;**167**:3463–3469.
21. Martos R, Baugh J, Conlon C, Patle A, Donnelly SC, McDonald K *et al.* Diastolic heart failure: evidence of increased myocardial collagen turnover linked to diastolic dysfunction. *Circulation* 2007;**115**:888–895.
22. Choudhuri R, Zhang HT, Donini S, Ziche M, Bicknell R. An angiogenic role for the neurokines midkine and pleiotrophin in tumorigenesis. *Cancer Res* 1997;**57**:1814–1819.
23. Owada K, Sanjo N, Kobayashi T, Muramatsu H, Muramatsu T, Michizawa M *et al.* Midkine inhibits caspase-dependent apoptosis via the activation of mitogen-activated protein kinase and phosphatidylinositol 3-kinase in cultured neurons. *J Neurochem* 1999;**73**:2084–2092.
24. Qi M, Ikematsu S, Ichihara-Tanaka K, Sakuma S, Muramatsu H, Muramatsu T *et al.* Midkine rescues Wilms' tumor cells from cisplatin-induced apoptosis: regulation of Bcl-2 expression by midkine. *J Biochem* 2000;**127**:269–277.
25. Sharov VG, Sabbah HN, Lesch M, Goldstein S. Evidence of cardiocyte apoptosis in myocardium of dogs with chronic heart failure. *Am J Pathol* 1996;**148**:141–149.
26. Chen C, Ma L, Linfelt DR, Lai T, Fallon JT, Gillam LD *et al.* Myocardial cell death and apoptosis in hibernating myocardium. *J Am Coll Cardiol* 1997;**30**:1407–1412.
27. Patten RD, Pourati I, Grohe C, Force T, Mendelsohn ME, Karas RH *et al.* 17β-estradiol reduces cardiomyocyte apoptosis in vivo and in vitro via activation of phospho-inositide-3 kinase/Akt signaling. *Circ Res* 2004;**95**:692–699.
28. He Z, Opland DM, Kulkarni RN, Wang B, Liao R, Kahn CR *et al.* Regulation of vascular endothelial growth factor expression and vascularization in the myocardium by insulin receptor and PI3K/Akt pathways in insulin resistance and ischemia. *Arterioscler Thromb Vasc Biol* 2006;**26**:787–793.
29. Yang Y-H, Wang Y, Zhang J, Zhu W, Wu D, Xu A *et al.* Suppression of the Raf/MEK/ERK signaling cascade and inhibition of angiogenesis by the carboxyl terminus of angiopoietin-like protein 4. *Arterioscler Thromb Vasc Biol* 2008;**28**:835–840.
30. Khan M, Varadharaj S, Parinandi NL, Tridandapani S, Kutala VK, Kuppusamy P *et al.* C-phycocyanin protects against ischemia-reperfusion injury of heart through involvement of p38 MAPK and ERK signaling. *Am J Physiol Heart Circ Physiol* 2006;**290**:H2136–H2145.
31. Zhao Z-Q, Budde JM, Velez DA, Muraki S, Guyton RA, Johansen JV *et al.* Adenosine attenuates reperfusion-induced apoptotic cell death by modulating expression of Bcl-2 and Bax proteins. *J Mol Cell Cardiol* 2001;**33**:57–68.
32. Rich T, Watson CJ, Wyllie A. Apoptosis: the germs of death. *Nat Cell Biol* 1999;**1**:69–71.
33. Liu Q, Muruve DA. Molecular basis of the inflammatory response to adenovirus vectors. *Gene Ther.* 2003;**10**:935–939.

Neuroscience 164 (2009) 1685–1694

HNK-1 (HUMAN NATURAL KILLER-1) GLYCO-EPITOPE IS ESSENTIAL FOR NORMAL SPINE MORPHOGENESIS IN DEVELOPING HIPPOCAMPAL NEURONS

I. MORITA,[a1] S. KAKUDA,[b1] Y. TAKEUCHI,[b] T. KAWASAKI[c] AND S. OKA[b*]

[a]*Department of Biological Chemistry, Graduate School of Pharmaceutical Sciences, Kyoto University, Kyoto 606-8501, Japan*

[b]*Department of Biological Chemistry, Human Health Sciences, Graduate School of Medicine, Kyoto University, Kyoto 606-8507, Japan*

[c]*Research Center for Glycobiotechnology, Ritsumeikan University, Shiga 525-8577, Japan*

Abstract—The human natural killer-1 (HNK-1) glyco-epitope possesses a unique structural feature, a sulfated glucuronic acid attached to lactosamine on the non-reducing termini of glycans. The expression of HNK-1 is temporally and spatially regulated by glucuronyltransferase (GlcAT-P) in the brain. Our previous report showed that mice lacking GlcAT-P almost completely lost HNK-1 expression in the brain and exhibited reduced long-term potentiation (LTP) at hippocampal CA1 synapses. GlcAT-P-deficient mice also showed impaired hippocampus-dependent spatial learning. Although HNK-1 plays an essential role in synaptic plasticity and memory formation, it remains unclear how HNK-1 regulates these functions. In this study, we showed that loss of the HNK-1 epitope resulted in an increase of filopodium-like immature spines and a decrease of mushroom-like mature spines in both the early postnatal mouse hippocampus and cultured hippocampal neurons. However, HNK-1 had no influence on spine density or filopodium formation. Immunofluorescence staining revealed that loss of HNK-1 altered the distribution of postsynaptic proteins such as α-amino-3-hydroxy-5-methylisoxazolepropionate (AMPA)-type glutamate receptor subunit GluR2 and PSD-95 from spine heads onto dendritic shafts without affecting synapse formation, resulting in an increase of shaft synapses in cultured GlcAT-P-deficient neurons. GluR2, a major HNK-1 carrier glycoprotein in postsynaptic density, has the ability to promote spine morphogenesis. Overexpression of GluR2 promoted spine growth in both wild-type and GlcAT-P-deficient neurons, but the increase in GlcAT-P-deficient neurons was lower than that in wild-type neurons. This is the first evidence that HNK-1 is a key factor for normal dendritic spine maturation and is involved in the distribution of postsynaptic proteins.

Key words: filopodium, glucuronyltransferase (GlcAT-P), GluR2, shaft synapse, spine maturation.

Glycosylation is one of the major post-translational protein modifications, especially for cell surface and secreted proteins, which play important roles in a variety of cellular functions (Ohtsubo and Marth, 2006). Several of the carbohydrates that are characteristically expressed on glycoproteins in the nervous system regulate synaptic plasticity (Kleene and Schachner, 2004). Among them, human natural killer-1 (HNK-1) is a well-characterized glyco-epitope found in the nervous system (Morita et al., 2008). HNK-1 is highly expressed in the brain during the early postnatal period, when the neural circuit is being actively formed. This epitope is carried by a series of cell adhesion molecules belonging to the immunoglobulin family cell adhesion molecules (NCAM, L1, P0, etc.) and extracellular matrix proteins (tenascin-R, phosphacan, etc.) (Saghatelyan et al., 2000; Liedtke et al., 2001). The HNK-1 glyco-epitope possesses a unique structure comprising a sulfated trisaccharide (HSO_3-3GlcAβ1-3Galβ1-4GlcNAc-) and is sequentially biosynthesized by one of two glucuronyltransferases (GlcAT-P or GlcAT-S) (Terayama et al., 1997; Seiki et al., 1999) and a sulfotransferase (HNK-1ST) (Bakker et al., 1997). To investigate the biological function of the HNK-1 epitope *in vivo*, we generated mice deficient in GlcAT-P, which is a major enzyme accounting for the majority of glucuronyltransferase activity in the nervous system (Yamamoto et al., 2002). The GlcAT-P-deficient mice showed an almost complete loss of HNK-1 expression in their brains and exhibited reduced long-term potentiation (LTP) at Schaffer collateral-CA1 synapses along with defects in spatial memory formation. Similarly, HNK-1ST-deficient mice also showed a reduction in LTP and abnormalities in spatial learning tasks (Senn et al., 2002). Recently, mice deficient in β4-galactosyltransferase-2 (β4GalT2), which is involved in Galβ1-4GlcNAc synthesis, were shown to exhibit markedly decreased HNK-1 expression as well as learning/memory impairment (Yoshihara et al., 2009). Although these lines of evidences strongly suggest that the HNK-1 epitope is essential for long-lasting changes in synaptic transmission, little is known about how HNK-1 modulates neural function.

Dendritic spines are highly specialized actin-rich small protrusions on neuronal dendrites and act as receptive sites for excitatory synaptic transmission. The size and number of spines are associated with synaptic plasticity including LTP and long-term depression (LTD), and it is considered that spine morphology is crucial for learning and memory (Segal, 2005). There are several different views on the origin of dendritic spines. One model is that spines initially form as dynamic filopodium-like protrusions and that these structures are then converted directly to

[1] These two authors equally contributed.

*Corresponding author. Tel: +81-75-751-3959; fax: +81-75-751-3959.
E-mail address: shogo@hs.med.kyoto-u.ac.jp (S. Oka).

Abbreviations: AMPA, α-amino-3-hydroxy-5-methylisoxazolepropionate; DiI, 1,1′-dioctadecyl-3,3,3′,3′-tetramethylindocarbocyanine perchlorate; DIV, days in vitro; Gal, galactose; GalT, galactosyltransferase; GlcA, glucuronic acid; GlcAT, glucuronyltransferase; GlcNAc, *N*-acetylglucosamine; GluR, glutamate receptor; HNK-1, human natural killer-1; HNK-1ST, HNK-1 sulfotransferase; LTP, long-term potentiation; PBS, phosphate-buffered saline; PSD, postsynaptic density; SDS, sodium dodecyl sulfate.

0306-4522/09 $ - see front matter © 2009 IBRO. Published by Elsevier Ltd. All rights reserved.
doi:10.1016/j.neuroscience.2009.09.065

mature spines, coincident with the process of postsynaptic specialization (Dailey and Smith, 1996; Ziv and Smith, 1996; Hering and Sheng, 2001). Another model is that dendritic spines arise from synapses located on dendritic shafts (shaft synapse) (Boyer et al., 1998; Fiala et al., 1998). AMPA type glutamate receptors mediate most of the fast excitatory synaptic transmission in the mammalian brain and control synaptic strength (Derkach et al., 2007; Isaac et al., 2007). The abundance of postsynaptic AMPA receptors is closely related to the size of dendritic spine heads and synapses, and their distributions regulate long-lasting synaptic changes. AMPA receptors are heterotetrameric complexes composed of various combinations of four subunits (GluR1–4). All subunits have an amino-terminal extracellular domain where four to six potential *N*-glycosylation sites are located (Pasternack et al., 2003). Among them, the extracellular domain of GluR2 has the ability to increase spine size and density in hippocampal neurons (Passafaro et al., 2003). The extracellular domain of GluR2 has four potential *N*-glycosylation sites, and the HNK-1 glyco-epitope is selectively expressed on the GluR2 subunit (Morita et al., in press).

In the present study, we showed that GlcAT-P-deficient mice had a large number of filopodium-like immature spines on their pyramidal neurons during the early postnatal period. However, filopodium sprouting and spine density were not affected by loss of the HNK-1 epitope. These observations indicate that HNK-1 plays an important role in the spine maturation process during conversion from filopodia to mature spines in a developmental stage-specific manner. Moreover, loss of HNK-1 also caused clustering of GluR2 and postsynaptic components on dendritic shafts instead of spine heads, indicating that abundant shaft synapses were formed. Our findings suggest that the HNK-1 glyco-epitope modulates the function of GluR2, resulting in normal spine morphogenesis in hippocampal neurons.

EXPERIMENTAL PROCEDURES

DNA constructs

The following mammalian expression plasmids were used: Venus (a GFP variant) attached to a membrane-targeted palmitoylation signal of GAP-43 (pCAGGS-GAP-Venus) was kindly provided by Drs. Y. Yoshihara and A. Miyawaki (RIKEN Brain Science Institute, Wako, Saitama, Japan) (Matsuno et al., 2006). GAP-Venus was released from pCAGGS-GAP-Venus with *Eco*RI and cloned into multi-cloning site A of the pIRES vector (Clontech, Mountain View, CA, USA). Then GlcAT-P was released from pEF-BOS-GlcAT-P (Terayama et al., 1997) with *Not*I and inserted into multi-cloning site B to yield pIRES-GAP-Venus-GlcAT-P. The 3.2 kb *Xho*I-*Xba*I GluR2 fragment derived from pKC24 (pBluescript) −GluR2, which was kindly provided by Dr. M. Mishina (Tokyo University, Tokyo, Japan) (Sakimura et al., 1990), was cloned into pcDNA3.1/myc-HisB (Invitrogen, Carlsbad, CA, USA) to yield the plasmid pcDNA3.1-GluR2.

DiI labeling

Mouse brains (n=3 for each genotype) were fixed in 4% paraformaldehyde in phosphate-buffered saline (PBS) and sectioned into 100 μm slices using a vibratome (Leica Microsystems, Wetzlar, Germany). 1,1′-dioctadecyl-3,3,3′,3′-tetramethylindocarbocyanine perchlorate (DiI) crystals (Molecular Probes, Eugene, OR, USA), a lipophilic tracer, were placed near the cell bodies of hippocampal CA1 pyramidal neurons to retrogradely label their dendrities. After 2 days, DiI diffusion on the pyramidal cell membrane was traced using confocal Z-series images taken at 0.75 μm depth intervals with the FLUOVIEW imaging system (OLYMPUS, Tokyo, Japan).

Cell cultures and transfection

Primary hippocampal cultures were prepared from postnatal day 0 mouse brains. Hippocampi were trypsinized for 10 min at 37 °C. Dissociated neurons were plated at 1.0×10^5 cells per well (BD BioCoat Poly-D-Lysine Cellware 4-Well CultureSlide (BD Biosciences, San Jose, CA, USA) coated with 2 μg/ml laminin) in Neurobassal medium (Gibco BRL, Grand Island, NY, USA) supplemented with 2% B27 (Gibco BRL) and 500 μM L-glutamine. Every 7 days, the cultures were fed by replacing half the medium with feeding medium. Hippocampal neurons were transfected using the MBS Mammalian Transfection Kit (Stratagene, La Jolla, CA, USA).

Immunostaining and antibodies

Cultured neurons were fixed in ice-cold methanol at −20 °C and then washed with PBS. Neurons were incubated with 3% bovine serum albumin in PBS containing primary antibodies for 1 h at room temperature. HNK-1 monoclonal antibody (a hybridoma cell line was purchased from the American Type Culture Collection, Manassas, VA, USA), anti-GFP (Nacalai Tesque, Kyoto, Japan), anti-PSD-95 (Upstate, Lake Placid, NY, USA), and anti-synaptophysin (FabGennix Inc., Frisco, TX, USA), anti-MAP-2 (Santa Cruz Biotechnology, Santa Cruz, CA, USA), and anti-GluR2 N-term antibodies (Zymed, San Francisco, CA, USA) were used. Alexa 448 and 546 secondary antibodies (Molecular Probes) were used for visualization. To label cytoskeletal F-actin, the neurons were fixed for 5 min in acetone at −20 °C and then stained with Alexa Fluor 546 Phalloidine (Molecular Probes).

Immunoprecipitation and immunoblot analysis

Cultured hippocampal neurons were lysed with 1 vol of 10 mM Tris–HCl (pH 7.4) buffer containing 1% sodium dodecyl sulfate and boiled for 5 min, and then five volumes of immunoprecipitation buffer (20 mM Tris–HCl (pH 7.4), 2% Triton X-100, and 0.3 M NaCl) and four volumes of H_2O were added to the lysate. To immunoprecipitate the GluR2 subunit, 4 μg/ml anti-GluR2/3 antibody (Upstate) and 20 μl of Protein G Sepharose 4 Fast Flow beads (GE Healthcare, Piscataway, NJ, USA) were added into the lysate and rotated for 2 h at 4 °C. Immunoblot analysis was performed using standard protocols.

Image analysis and quantification

For the DiI labeling experiments, neurons were chosen randomly from three independent littermate pairs. For the analysis of GFP-transfected neurons, neurons were chosen from three to five independent experiments. Morphological analysis was carried out using MetaMorph image analysis software (Molecular Devices, Sunnyvale, CA, USA). The length and width of the protrusions along dendrites were measured. Spines and filopodia were classified as follows: spines were defined as 0.5–1.5 μm length protrusions with mushroom-like heads, and filopodia were defined as protrusions longer than 1.5 μm without spine heads. In the case of GluR2 overexpression experiments, spines were defined as 0.5–2.0 μm length protrusions with mushroom-like heads, and filopodia were defined as protrusions longer than 2.0 μm without spine heads because of the unusual large spine heads. The densities of protrusions, spines and filopodia are indicated as their number per 10 μm of dendrite.

Statistical analysis

The statistical analyses performed are listed in the individual figure legends, and values are expressed as the mean ± standard error of the mean (SEM).

RESULTS

Loss of the HNK-1 glyco-epitope affects the dendritic spine morphology of pyramidal neurons

The expression of the HNK-1 glyco-epitope is developmentally regulated in the nervous system and peaks between postnatal days 7 (P7) and P14, which corresponds to the period of neural circuit formation. To examine if the loss of the HNK-1 epitope resulted in abnormalities in neuronal structure, the hippocampal neurons of brain slices prepared from wild-type and GlcAT-P-deficient mice at P14 were visualized by Golgi staining. Compared to wild-type, the overall organization and development of the dendritic trees of individual CA1 pyramidal neurons in the hippocampus appeared relatively normal in the GlcAT-P-deficient mice. Close observation showed that thinner brush-like protrusions were found in GlcAT-P-deficient than in wild-type mice slices (Supplementary Fig. 1).

To analyze the neuronal fine structure in GlcAT-P-deficient mice, we prepared hippocampal slices and visualized CA1 pyramidal neurons by DiI labeling. At P14, most pyramidal neurons in wild-type mice possessed mature spines with mushroom-like heads (Fig. 1A, arrowheads); whereas, the majority of dendritic protrusions were immature filopodium-like spines in GlcAT-P-deficient mice (Fig. 1A, arrows). To quantify the differences in spine morphology, the lengths, widths, and densities of the protrusions were measured. Cumulative frequency plots obtained from three respective littermates revealed that the distribution of the lengths of the protrusions in GlcAT-P-deficient mice showed a significant shift toward longer lengths, and the distribution of the widths shifted toward thinner widths (Fig. 1B). The mean length of GlcAT-P-deficient mice increased to 136.8% of that of wild-type mice (Fig. 1B, left panel inset, and Table 1, * $P<0.05$), and the mean width decreased to 87.7% of that of wild-type (Fig. 1B, right panel inset, and Table 1, * $P<0.05$). However, the protrusion density was not significantly different between the two groups (Fig. 1C, Table 1, $P=0.59$). In addition, we classified the protrusions into mature spines and filopodia according to the criteria described in Experimental procedures. As shown in Fig. 1C, 75.6%±2.1% of dendritic protrusions were mature spines in wild-type mice, but only 43.7%±1.8% were in GlcAT-P-deficient mice (** $P<0.01$).

In adult mice (P70), most of the dendritic protrusions had grown into mature spines in both wild-type and GlcAT-P-deficient mice (Fig. 1D). There were no differences in length (wild-type, 1.05±0.03 μm; GlcAT-P −/−, 1.17±0.01 μm, $P=0.49$) and width (wild-type, 0.71±0.02 μm; GlcAT-P −/−, 0.69±0.02 μm, $P=0.58$) (Fig. 1E, Table 1). The proportion of mature spines was 83.8±6.8% in GlcAT-P-deficient mice, compared to 91.5±1.0% in wild-type mice (Fig. 1F, Table 1, $P=0.41$). These results suggest that mice lacking HNK-1 exhibit the impairment of spine morphology in the developing brain.

Loss of HNK-1 impairs the maturation of spines in cultured hippocampal neurons

To address the effect of HNK-1 on spine morphology in detail, we prepared cultured hippocampal neurons. We transfected GFP at 15 days in vitro (DIV) and then visualized spine morphology at 18 DIV. At this stage, wild-type neurons showed robust spine formation, and the immunoreactivity against HNK-1 antibody was diffusely distributed on dendritic shafts and spine heads (Fig. 2A, left, arrowheads). In contrast, GlcAT-P-deficient neurons had many long, thin protrusions extending from dendrites without enlarged spine heads (Fig. 2A, middle). Quantitative analysis showed that the mean length of the protrusions in GlcAT-P-deficient neurons increased to 133.5% of that in wild-type neurons (Fig. 2B, upper panel inset and Table 2, ** $P<0.01$), and the mean width decreased to 75.0% of that in wild-type neurons (Fig. 2B, lower panel inset, and Table 2, ** $P<0.01$). However, no significant difference in the protrusion density was observed (Fig. 2C). The proportion of mature spines among all dendritic protrusions was 46.7±1.3% and 75.8±1.5% in GlcAT-P-deficient and wild-type neurons, respectively (Fig. 2C, ** $P<0.01$). These data were consistent with the results obtained from hippocampal slices (Fig. 1), indicating that loss of the HNK-1 epitope also caused significant impairment of spine morphogenesis in cultured hippocampal neurons. On further close observation, we found that the remaining filopodia in GlcAT-P-deficient neurons did not show an irregular appearance. The length was almost always within the range from 1.5 to 3.3 μm, which is considered to represent normal filopodia in immature neurons (3.3±1.1 μm) (Zhang and Macara, 2006). We hypothesized that loss of HNK-1 leads to inhibition of the conversion of filopodia to mature spines, rather than the sprouting of filopodia. To examine this idea, we examined the morphology of 12 DIV neurons. Wild-type neurons at 12 DIV had elaborated dendrites and filopodia, but did not have mature spines (Fig. 3A). As expected, the quantitative analysis showed that at this time point both wild-type and GlcAT-P-deficient neurons exhibited normal filopodia morphology with mean lengths of 3.23±0.22 and 3.20±0.12 μm, respectively ($P=0.93$), and no significant difference in the density of filopodia (wild-type, 4.14±0.06; GlcAT-P −/−, 4.35±0.27, $P=0.51$) (Fig. 3B, Table 2). Taken together, these results indicate that loss of HNK-1 results in the inhibition or retardation of spine maturation in cultured hippocampal neurons by affecting the later step(s) of spine morphogenesis (at least after 12 DIV).

Immature spine morphology in GlcAT-P-deficient neurons is rescued by GlcAT-P expression

To examine whether the altered spine morphology was restored by the re-expression of HNK-1, we co-transfected GFP and GlcAT-P expression plasmids into GlcAT-P-deficient neurons at 15 DIV and then analyzed spine morphology. At 18 DIV (3 days after GlcAT-P transfection), the spine morphology in GlcAT-P-deficient neurons was res-

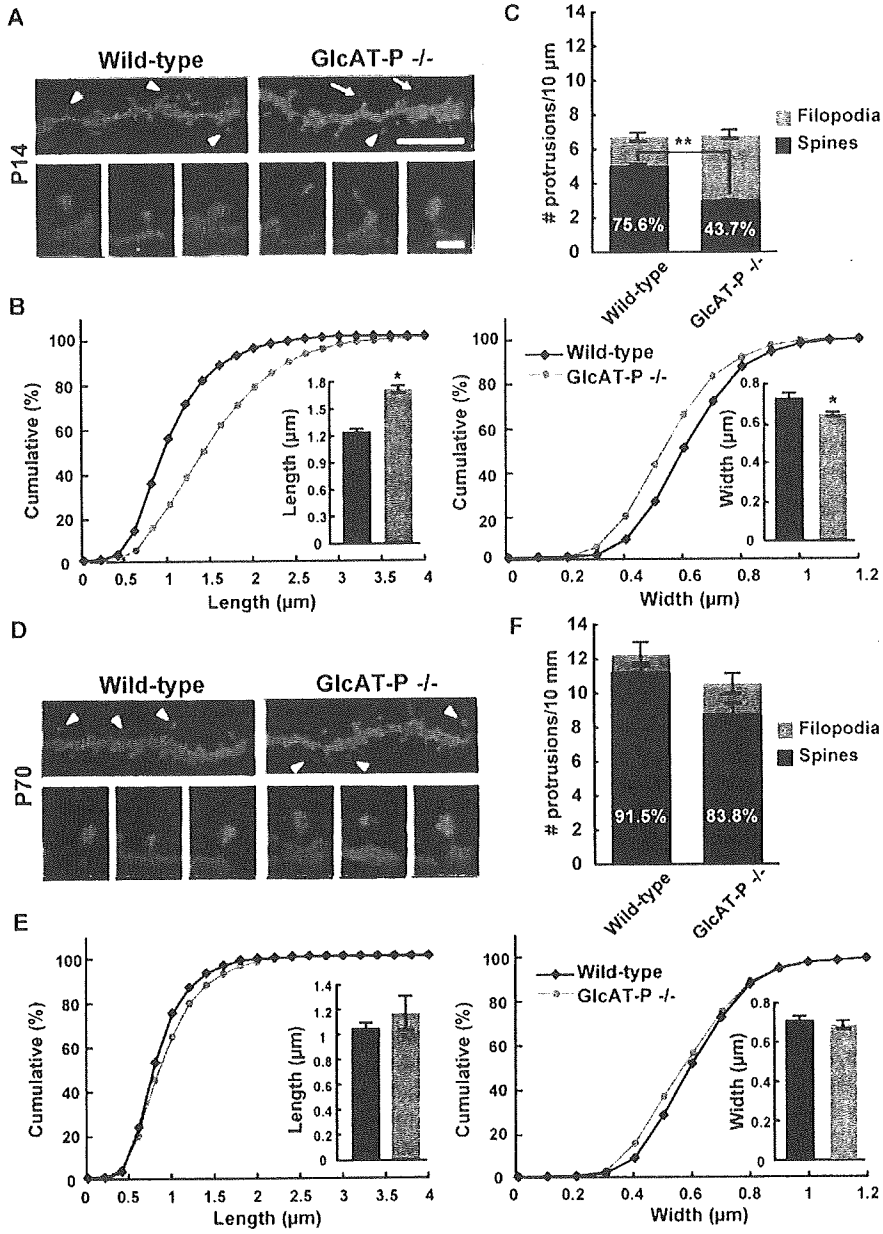

Fig. 1. Impaired spine morphology of pyramidal neurons in GlcAT-P-deficient (GlcAT-P −/−) hippocampal slices. (A) Representative images of DiI-labeled apical dendrites of CA1 pyramidal neurons in hippocampal slices from P14 wild-type and GlcAT-P −/− mice. Arrowheads indicate dendritic spines, and arrows indicate filopodia. Scale bars: 10 μm in the upper panel and 1 μm in the lower panel. (B) Cumulative frequency plots of the length and width of dendritic protrusions (n=1090 protrusions for wild-type neurons; n=1147 protrusions for GlcAT-P −/− neurons). P<0.01 (Kolmogorov–Smirnov Test). Inset histograms show mean values (n=3, 276–498 protrusions per experiment for wild-type neurons; n=3, 247–465 protrusions per experiment for GlcAT-P −/− neurons). * P<0.05 (two-tailed t-test). (C) The densities of protrusions in (B) (n=3, 13–15 cells per experiment for wild-type neurons; n=3, 13–17 cells per experiment for GlcAT-P −/− neurons). The numbers on the bars indicate the percentages of mature mushroom-like spines within all protrusions. ** P<0.01 (two-tailed t-test). (D) Representative images of DiI-labeled apical dendrites of CA1 pyramidal neurons in hippocampal slices from P70 wild-type and GlcAT-P −/− mice. (E) Cumulative frequency plots of the length and width of dendritic protrusions at P70 (n=927 protrusions for wild-type neurons; and n=970 protrusions for GlcAT-P −/− neurons). Inset histograms show mean values (n=3, 294–450 protrusions per experiment for wild-type neurons; and n=3, 235–388 protrusions per experiment for GlcAT-P −/− neurons). (F) The densities of protrusions in (E) (n=3, 8–9 cells per experiment for wild-type neurons; n=3, 8–10 cells per experiment for GlcAT-P −/− neurons). Error bars indicate SEM. For interpretation of the references to color in this figure legend, the reader is referred to the Web version of this article.

cued by GlcAT-P transfection (Fig. 2A, right panel), and HNK-1 staining were also observed on dendritic shafts and spine heads (Fig. 2A, right panel, arrowheads). The mean length and width of dendritic protrusions reached 97.7%